



Tracing the peak of Neoglacial cooling on the Western Antarctic Peninsula: The Little Ice Age moraines of Marguerite Bay

Attila Çiner^{a,*}, Cengiz Yıldırım^a, M. Akif Sarıkaya^a, Yohanna Klanten^b, Marc Oliva^c, Yeong Bae Seong^d, Byung Yong Yu^e

^a Eurasia Institute of Earth Sciences, İstanbul Technical University, Maslak, İstanbul, Türkiye

^b Department of Geography, Centre for Northern Studies (CEN) and Takuvi International Research Laboratory, Université Laval, QC, Canada

^c Department of Geography, Universitat de Barcelona, Spain

^d Department of Geography Education, Korea University, Seoul, 02841, South Korea

^e Laboratory of Accelerator Mass Spectrometry, Korea Institute of Science and Technology, Seoul, 02792, South Korea

ARTICLE INFO

Handling Editor: Bethan Davies

Keywords:

Neoglacial
Little ice age
Antarctic peninsula
Marguerite bay
Horseshoe island
Calmette peninsula
Moraines
Cosmogenic surface exposure dating
Paleoclimate

ABSTRACT

Constraining the timing of glacial advances and retreats is crucial for understanding paleoclimate and forecasting future trends. While the retreat of the western side of the Antarctic Peninsula ice sheet since the Last Glacial Maximum (*ca.* 26–19 ka) is relatively well-documented, the Neoglacial period (*ca.* 4 to 0.2 ka), primarily represented by moraine and lacustrine records, remains poorly constrained. In this study, we compiled a non-exhaustive list of potentially datable, fresh-looking moraines located near active glaciers along Marguerite Bay, the largest bay in the Western Antarctic Peninsula. Subsequently, we utilised ^{10}Be Terrestrial Cosmogenic Nuclide (TCN) surface exposure dating on three moraine complexes adjacent to three distinct glaciers: the Shoesmith and Erinç moraines on Horseshoe Island and the Erol Moraine on the Calmette Peninsula. The results from boulders, cobbles, and pebbles ($n = 9$) of the Shoesmith lateral moraine yielded a mean exposure age of 496 ± 79 years, coinciding with the Little Ice Age (LIA) in the Northern Hemisphere and marking the end of the Neoglacial period. The boulders ($n = 4$) collected from the right lateral moraine of the Erinç Glacier, which consists of several recessional ridges, are challenging to interpret owing to significant age scatter. Multiple scenarios indicate a late Neoglacial advance with an error-weighted mean landform age of 1163 ± 403 years. We also tentatively attribute the formation of the undated innermost moraine ridge, located just a few tens of metres from the current glacier front, to the LIA. The moraine boulders ($n = 3$) collected from the youngest end moraine of the Erol Glacier exhibit significant inheritance, with unusually high ages ranging from *ca.* 2 to 10 ka. This is likely due to limited subglacial erosion of boulders and/or short supraglacial transport, which do not permit the zeroing of previously accumulated nuclides. Nevertheless, the cross-cutting relationships between the Erol Moraine that overlie previously OSL- and ^{10}Be -TCN-dated raised beaches indicate its formation during the LIA advance. We also highlight the complexities associated with asynchronous moraine formation and inheritance in glacial boulders that experience low rates of erosion. Overall, our data refine the chronology of the late Neoglacial period on the Western Antarctic Peninsula, highlighting the significance of the LIA in a region where its timing and duration had previously remained unclear.

1. Introduction

Following the Holocene Thermal Maximum (Renssen et al., 2009, 2012), the Neoglacial (*ca.* 4 to 0.2 ka ago) was one of the most unstable cooling periods, culminating in the Little Ice Age (LIA), which is generally accepted to have occurred between *ca.* 1300 and 1850 CE (Miller et al., 2012). The LIA is considered a modest cooling of the

Northern Hemisphere, accompanied by a temperature decrease of less than 1 °C relative to late 20th-century levels (Mann et al., 1998). This cooling was frequently linked to glacier growth in both hemispheres. However, while cooling in Antarctica may occur at the same time as in the Northern Hemisphere, the factors driving these changes may differ (see Simms et al. (2021) for a discussion on the drivers and rates of paleoclimate changes in Antarctica). Numerous studies suggest that the

* Corresponding author.

E-mail address: cinert@itu.edu.tr (A. Çiner).

LIA in Antarctica was both colder (up to *ca.* -2°C) and stormier than it is today, with climate conditions broadly aligning with global patterns (e.g., Bertler et al., 2011; Li et al., 2009; Orsi et al., 2012). During the post-LIA warming period, temperatures across the Antarctic Peninsula increased significantly, making it one of the fastest-warming regions on Earth (Turner et al., 2014). However, recent decades have also experienced periods of cooling (Oliva et al., 2017). Therefore, constraining the response of ice masses in the Antarctic Peninsula to LIA cooling is essential for understanding the factors and rates of paleoclimate change and, consequently, for validating models of future glacier behaviour (Davies et al., 2014).

The Marguerite Bay region of the Western Antarctic Peninsula features several proglacial ice-free areas where moraines are exposed alongside active and often tidewater glaciers (Fig. 1). However, well-preserved glacial landforms are not always easy to locate as they are frequently submerged beneath the sea (e.g., Sarikaya et al., 2025). Batchelor et al. (2019) utilised high-resolution bathymetric data in Darbel Bay (*ca.* 140 km northeast of our study site on Horseshoe Island) to identify *ca.* 250 small (less than 1–3 m high, 10–20 m wide) and quite evenly spaced submarine recessional moraines outside the tidewater Philippa Glacier limit, indicating the slow withdrawal of a grounded ice

mass. Indeed, tidewater glaciers on the Western Antarctic Peninsula have experienced substantial termini retreat and flow acceleration due to amplified air and ocean temperatures since the onset of the Neoglacial period (e.g., Oliva et al., 2024), particularly during the past half-century (Vaughan et al., 2003; Cook et al., 2005, 2016; Molina et al., 2007; Oliva et al., 2024).

The online ICE-D Antarctica database (<https://ice-d.apps.pgc.umn.edu/antarctica/>; census date, June 2025) indicates that glacial deposits have been dated in only two areas using Terrestrial Cosmogenic Nuclides (TCN) throughout the entire Marguerite Bay region. A total of ten granitic erratic boulder TCN surface exposure ages collected from Pourquoi Pas Island (Bentley et al., 2011) and Horseshoe Island (Ciner et al., 2019) indicate a rapid deglaciation of the former Marguerite Trough Ice Stream (MTIS) at the onset of the Holocene (Ó Cofaigh et al., 2008, 2014; Bentley et al., 2006, 2011; Johnson et al., 2012).

There are no age constraints on the already limited TCN surface exposure for erratic boulders in the Marguerite Bay area. Surprisingly, Marguerite Bay and the entire Western Antarctic Peninsula suffer from a lack of dated moraines, except in the Southern Shetland Islands, where the Neoglacial record is patchy (e.g., Ingólfsson et al., 1998; Palacios et al., 2020; Oliva et al., 2023, 2024).

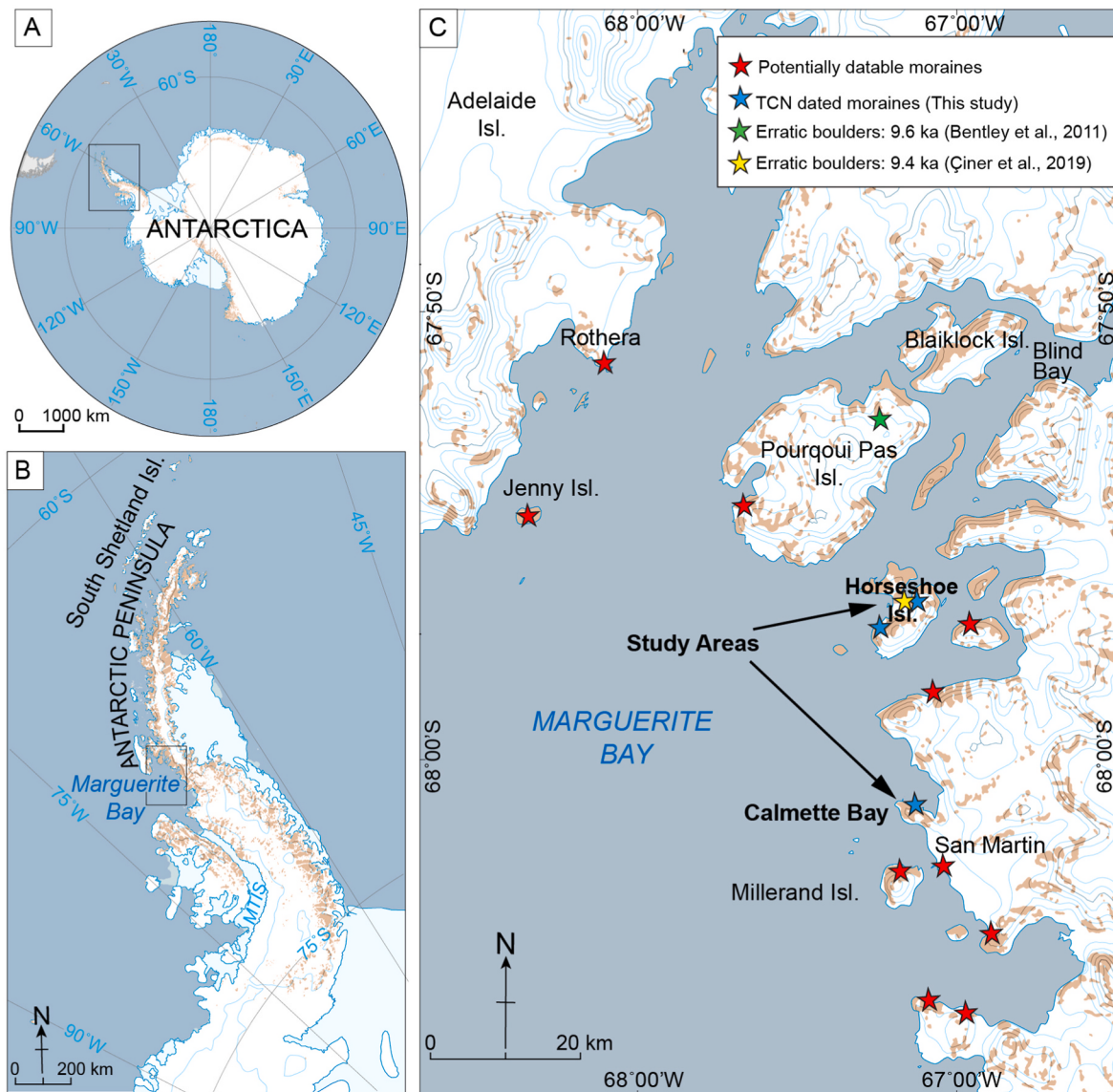


Fig. 1. Location of the A) Antarctic Peninsula, B) Marguerite Bay, and C) Study locations. Brown spots show ice-free areas. MTIS: Marguerite Trough Ice Stream (map adapted from Yıldırım, 2020). (For interpretation of the references to colour in this figure legend, the reader is referred to the Web version of this article.)

The primary goal of this study is to enhance our understanding of on-shore moraine development following the retreat of the Marguerite Trough Ice Stream from the Marguerite Bay region. By utilising remote sensing imagery alongside select field surveys, we initially present a non-exhaustive map highlighting moraines located along the coast (Fig. 1c). We have particularly focused on active glaciers that show signs of movement on Horseshoe Island and the Calmette Peninsula. We utilised ^{10}Be TCN surface exposure dating to analyse three moraine complexes adjacent to three distinct glaciers and to reveal the Marguerite Bay late Neoglacial and particularly LIA record. Our findings establish a basis for comparison with other late Neoglacial dates in the Western Antarctic Peninsula, thus contributing to a more comprehensive understanding of the region's glacial history and postglacial geomorphological dynamics.

2. Site descriptions

2.1. Marguerite Bay

Marguerite Bay, centred at $68^{\circ} 50' \text{S}$, $68^{\circ} 58' \text{W}$ ($220 \text{ km} \times 120 \text{ km}$), constitutes the largest embayment ($\text{ca. } 25.000 \text{ km}^2$) along the Western Antarctic Peninsula (Fig. 1). The eastern coast of the bay contains numerous tidewater glaciers and fjords. On-shore, lateral, and end moraines are observed, especially in the central and northern part of the bay area (Fig. 1c). In the south, the Marguerite Trough Ice Stream flowed north into Marguerite Bay and once covered the entire bay area during the Last Glacial Maximum, $\text{ca. } 26$ to 19 ka ago (Ó Cofaigh et al., 2014).

Cold maritime conditions characterise the current climate in Marguerite Bay. Meteorological data from the nearby British Rothera station (between 1977 and 2015) and the Argentine San Martín station (between 1985 and 2015) indicate mean annual air temperatures of -4.3°C and -4.6°C , respectively (Oliva et al., 2017). The mean annual precipitation is $\text{ca. } 500 \text{ mm}$ (Turner et al., 2020).

In Marguerite Bay, the glaciers that formed during the Last Glacial Cycle began retreating $\text{ca. } 14\text{--}13 \text{ ka BP}$ (Bentley et al., 2006; Kilfeather et al., 2011). ^{14}C dating from lakes and ^{10}Be TCN surface exposure ages from erratic boulders indicate a rapid retreat of the ice stream, which caused sea levels to rise and flood the inner part of the bay between 10 and 7 ka (Anderson and Oakes-Fretwell, 2008; Bentley et al., 2005a, 2011; Ó Cofaigh et al., 2008, 2014; Çiner et al., 2019; Hodgson et al., 2013; Livingstone et al., 2013).

Currently, there are no age data on glacial deposits from the Marguerite Bay area after 7 ka, which covers the Neoglacial period. However, ^{10}Be TCN ages from several raised beaches indicate a 15 m relative sea-level change over the past 3.31 ka on Horseshoe Island (Yıldırım et al., 2024). The authors also used ^{10}Be TCN to date other raised beaches in the Calmette Peninsula, located 20 km south of Horseshoe Island. They reported a 36 m relative sea-level fall over the last 7.29 ka, suggesting significant and differential glacial-isostatic adjustments in both regions during the middle and late Holocene. On the other hand, Simkins et al. (2013) used OSL dating to date the same raised beaches in the Calmette Peninsula and proposed a mid-Holocene (5.5–7.3 ka) marine limit at 21.7 m for the Marguerite Bay area.

2.2. Horseshoe Island

Horseshoe Island ($67^{\circ} 85' \text{S}$, $67^{\circ} 20' \text{W}$; $9 \times 10 \text{ km}$) is the third-largest island in the Marguerite Bay archipelago, covering $\text{ca. } 64 \text{ km}^2$, with a coastline extending 53.8 km (Tükenmez et al., 2022). Approximately two-thirds of the island is occupied by glaciers or semi-perennial ice and snow (Yıldırım, 2020) (Figs. 1 and 2).

The geology of Horseshoe Island consists of foliated granitic and banded gneisses from the Antarctic Peninsula Metamorphic Complex (Matthews, 1983). A Lower Jurassic age has recently been assigned to foliated and undeformed granites (Velev et al., 2023). The Antarctic Peninsula Volcanic Group comprises foliated volcanic rocks and

sediments (Matthews, 1983). Furthermore, the Andean Plutonic Suite includes several white and pink to brick-red coloured granitic intrusions, gabbro, and diorite of Cretaceous age (Loske et al., 1997).

The island's northern part features gentle topography, culminating in the pyramidal Mount Searle (537 m above sea level; asl). The British Antarctic Survey's Research Base Y, which operated between 1955 and 1960, is located near Sally Cove to the north. In contrast, the island's southern side is heavily glaciated and dominated by Mount Breaker (879 m asl).

Running from north to south, the island is divided by a narrow ($1 \text{ km} \times 1.5 \text{ km}$), mostly ice-free, flat-lying central col, $\text{ca. } 80\text{--}100 \text{ m asl}$ (Yıldırım, 2020). Five clear-water lakes are located in this area, with the largest (Col Lake 1) measuring $\text{ca. } 200$ by 60 m and reaching a depth of 3.2 m (Hodgson et al., 2013). Limnological and sedimentological studies, along with ^{14}C ages from Col Lake 1 (Hodgson et al., 2013) and ^{10}Be TCN surface exposure dating of well-polished and striated granitic erratic boulders (Çiner et al., 2019) on the col surface, indicate that part of the island became partially ice-free at $\text{ca. } 9.4 \text{ ka}$.

Some late Pleistocene landforms include stone polygons derived from frost-shattered rocks, erratic blocks on bedrock, moraine ridges, talus deposits along mountain fronts and cliffs, shingle beaches, and braided stream deposits. The col area slopes northeast toward Gaul Cove and southwest toward Lystad Bay, where the Shoesmith Glacier Moraine marks its southern boundary. Both bays feature shingle-raised beaches. A recent ^{10}Be TCN surface exposure dating study in Gaul Cove assessed four raised beaches at elevations ranging from 1.8 to 15 m asl, dating them to 0.26 to 3.31 ka, respectively (Yıldırım et al., 2024). The temporary Turkish Antarctic Research Station was established at the beach area of Lystad Bay in 2019.

2.2.1. Shoesmith Glacier and Moraine

Shoesmith Glacier ($67^{\circ} 84' \text{S}$ - $67^{\circ} 20' \text{W}$), $\text{ca. } 4 \text{ km long} \times 1.7 \text{ km wide}$, is the largest glacier on Horseshoe Island (Figs. 3 and 4). It originated from a composite cirque area east of the island at an elevation of $\text{ca. } 500 \text{ m asl}$. At $\text{ca. } 350 \text{ m asl}$, the glacier splits into two branches. The more active and prominent branch flows west into Lystad Bay, while the smaller and less active branch runs north and calves into Gaul Cove. The glacier's apparent lateral thickness is $\text{ca. } 15 \text{ m}$, while it reaches $\text{ca. } 20 \text{ m}$ in the calving area. The gravity survey conducted along the glacier's long axis indicates a thickness of up to $\text{ca. } 100 \text{ m}$ at its thickest part (Smith, 1973).

A main lateral moraine, stretching 1.5 km from Gaule Cove to Lystad Bay, exhibits an apparent thickness of $\text{ca. } 10 \text{ m}$. A few smaller recessional ridges are also observed at lower elevations. Although it is only $\text{ca. } 15 \text{ m wide}$ at both ends, it reaches $\text{ca. } 75 \text{ m}$ in the central part, at an elevation of 87 m asl. The moraine is detached from the glacier, and in two sections where it was observed, all grain sizes were clearly visible with no ice between the sediments. We therefore assumed this moraine to be a relict feature. The moraine comprises pink and white, rounded to sub-angular granitic pebbles (1–3 cm), rounded and platy cobbles (10–20 cm long and 5–8 cm thick), and sub-rounded to rounded, well-polished, hard granitic boulders that can reach diameters of up to 1 m. Although some other lithologies, such as dark-coloured gabbro and basic dyke pebbles, are encountered, they constitute less than 2 % of the sediments. A fine, sandy, and muddy matrix is also locally present between the coarser sediments. Another smaller lateral moraine, $\text{ca. } 500 \text{ m long}$, on the other side of the glacier, also extends to Gaule Cove, which we did not explore.

We collected a total of ten samples (four amalgamated samples in 2018 and six boulder samples in 2022) from the Shoesmith Moraine. The samples collected in 2022 consisted of solid white granite without fractures, which was extremely difficult to break. Therefore, samples Cosmo 1c and 2c were collected using an electric masonry drill (Fig. 4j). The Cosmo 2b sample, however, lacked enough quartz and was therefore not measured.

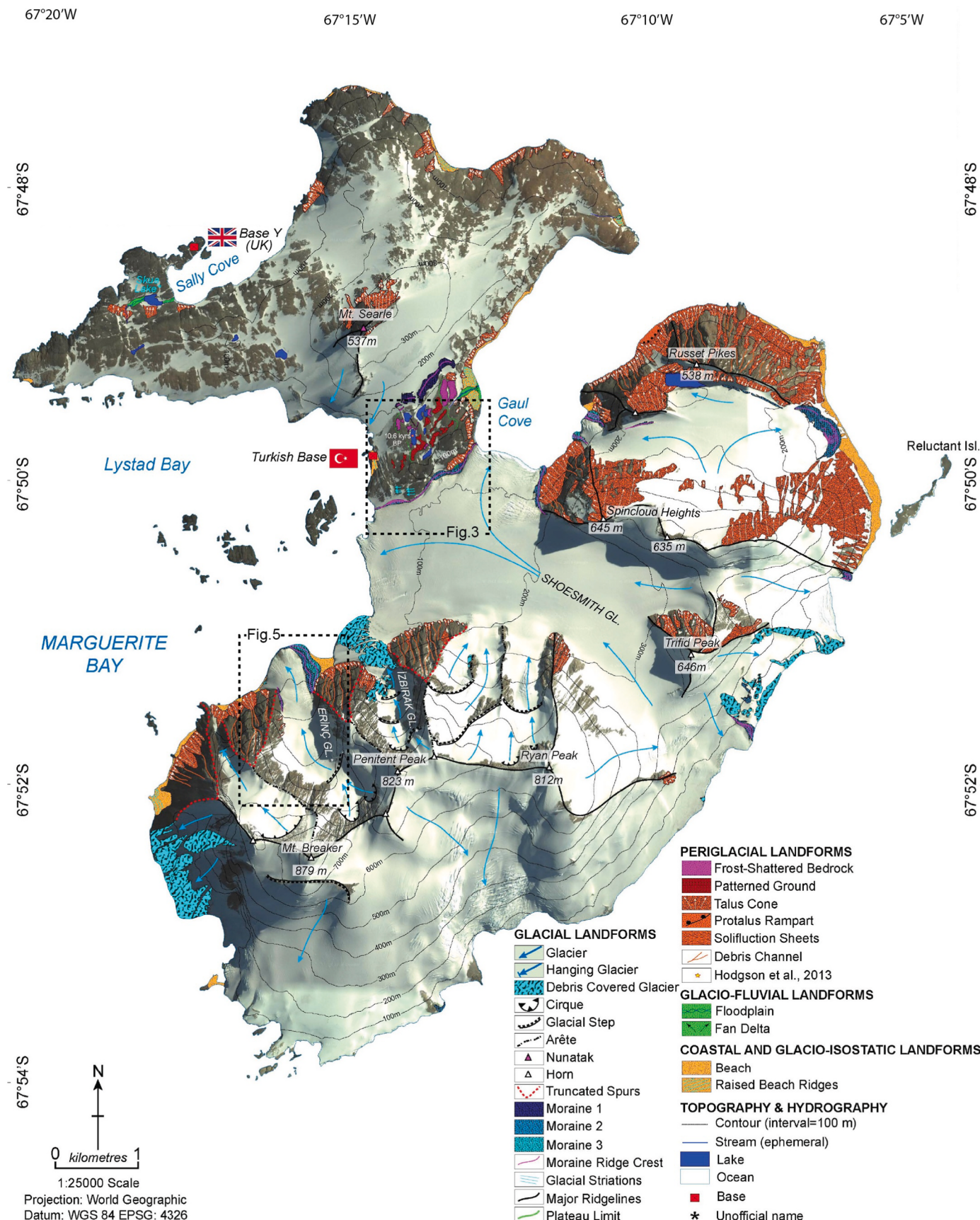


Fig. 2. A) Geomorphological map of the Horseshoe Island (adapted from Yıldırım, 2020). Figs. 3 and 5 locations are shown in boxes.

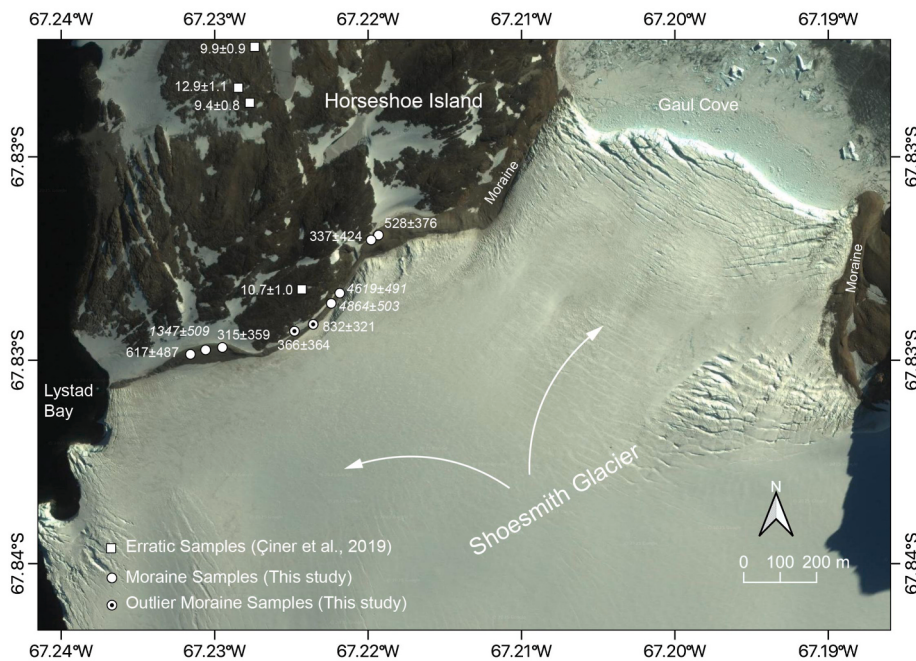


Fig. 3. Shoesmith Glacier and its moraines. Erratic granitic block samples (white squares) in the col area confirm the timing of ice-sheet retreat at 9.4 ± 0.8 ka (the youngest boulder age) (Ciner et al., 2019). The moraine boulder ages (white circles) are presented without their sample numbers for clarity. The error-weighted mean age of moraine samples yields 496 ± 79 years. See Fig. 2 for image location. The background image is taken from Google Earth.

2.2.2. Erinç Glacier and Moraine

The Erinç Glacier ($67^{\circ} 85'$ S— $67^{\circ} 26'$ W) is the second largest glacier on Horseshoe Island, measuring ca. 2.3 km long and 0.4–0.7 km wide (Figs. 5 and 6). Its apparent thickness ranges from ca. 15–25 m. The glacier is sourced from two small cirques located at ca. 750 m asl and flows from the southeast toward the northwest, calving at Lystad Bay.

A curved left lateral moraine, ca. 400 m long and 10–25 m wide, and a significantly larger right lateral moraine, which measures between 130 and 170 m in width and ca. 700 m in length, reaching Lystad Bay, are present. The right lateral moraine consists of several recessional ridges, each with an apparent height of ca. 10 m and a width of up to 20 m (Figs. 5 and 6).

During our fieldwork in 2018, the right lateral moraine ridges were covered in fresh snow, presenting a significant challenge in selecting the best sampling areas. Nevertheless, several smaller recessional ridges were visible in the clear summertime images on Google Earth. We selected the three youngest recessional ridges (M1 to M3; from oldest to youngest). We assumed the ridges were relict features because they are detached from the glacier with no ice between the sediments on the moraine sections, except possibly the closest ridge to the glacier, which we did not date. The moraine ridges consist of white angular to sub-angular granitic boulders ranging from 30 to 60 cm in diameter, along with smaller angular fragments and occasional boulders larger than 1 m. No rounded or polished boulders were encountered, unlike those found at the Shoesmith Moraine. Due to weather constraints, we sampled only the most prominent M1 and M2 moraines, collecting two samples from each feature.

2.3. Calmette Peninsula

Calmette Bay, centred at $68^{\circ} 04'$ S, $67^{\circ} 14'$ W (5×6 km), is a small fjord located on the mainland Antarctic Peninsula, ca. 20 km south of Horseshoe Island (Figs. 1 and 7). The southern part of the bay forms a small peninsula, ca. 5.5 km long and 2.5 km wide, oriented roughly from east to west, with a peak elevation of 384 m asl. The geology of Calmette Peninsula is similar to that of Horseshoe Island, comprising granitic intrusions, gabbro, and diorite, often cut by a few-meter-thick basic

dykes.

The peninsula's southern shore is steep and narrow, while the northern section, facing Calmette Bay, features ice-free areas. A small glacier, informally referred to here as the Erol Glacier in honour of the prominent Turkish geomorphologist Oğuz Erol, is located on the north side, along with its well-preserved terminal moraine complex (Figs. 8 and 9). Up to 30 well-developed raised shingle beaches reaching ca. 40 m asl are composed of poorly sorted and often rounded cobbles of granite and diorite (Bentley et al., 2005b; Hodgson et al., 2013; Simkins et al., 2013; Yıldırım et al., 2024). Additionally, very steep talus cones are observed along the northern shore, measuring between 100 and 150 m in height. On the eastern coast of Calmette Bay, a tidewater glacier with a steep calving face supplies the bay with icebergs.

2.3.1. Erol Glacier and Moraine

The Erol Glacier ($68^{\circ} 06'$ S – $67^{\circ} 18'$ W) is a small glacier measuring ca. 1.5 km long and 1 km wide (Figs. 8 and 9). It is sourced from two small cirques at ca. 230 m asl and flows from the southwest toward the northeast. Unlike the previously described tidewater glaciers, this is a land-terminating glacier located ca. 300 m from the shoreline, with two well-developed end moraine loops (M1 and M2) and a smaller, younger end moraine (M3) developed at ca. 100 m asl, all together forming a terminal moraine complex. Although we did not observe any ice between the boulders, M3 could be an active ice marginal feature, unlike M1 and M2, which are completely detached from the glacier lying at lower elevations.

Due to time constraints, we sampled only the youngest moraine (M3). The blocks are composed of granitic and dioritic rocks, ranging in thickness from 20 to 70 cm, with some exceeding 1 m. They are predominantly angular and appear very fresh and uneroded, lacking fine sediments.

3. Data and methods

3.1. Fieldwork and mapping

We initially conducted a reconnaissance survey of potential glacial

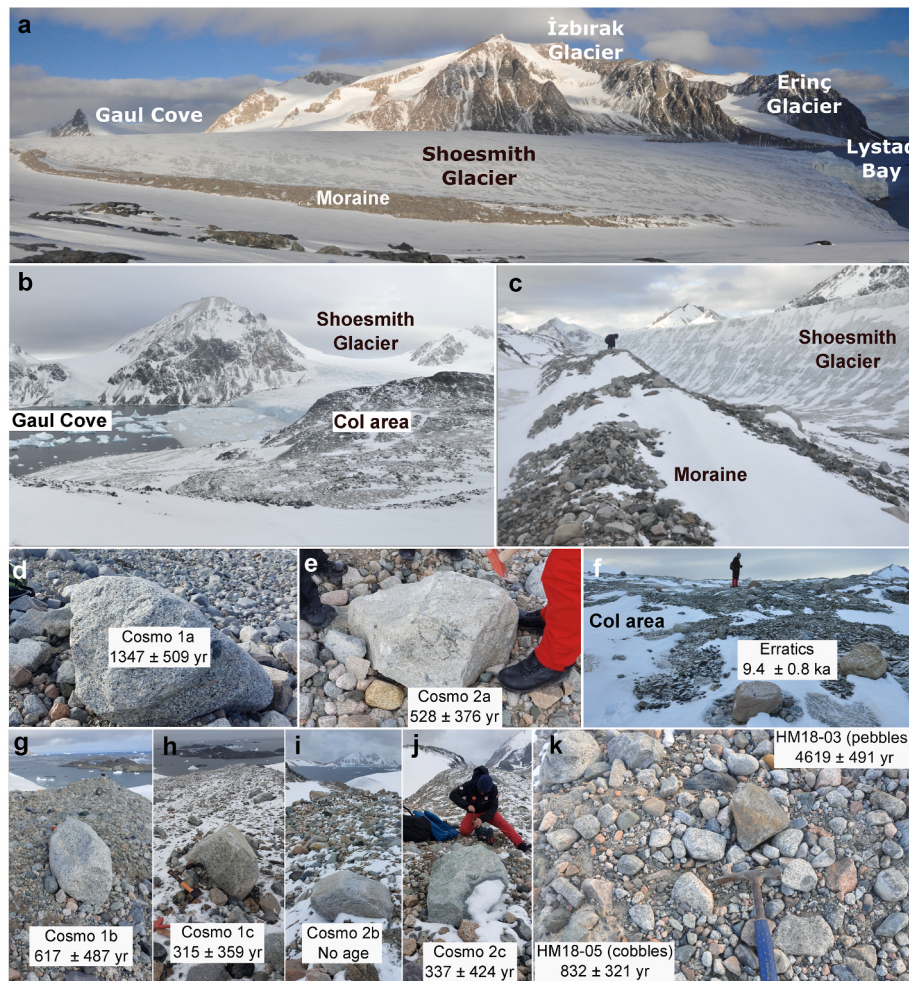


Fig. 4. a) General view of the Shoesmith and Erinç glaciers, featuring their respective lateral moraines, both calving into Lystad Bay; b) the opposite end of the Shoesmith Glacier calving into Gaule Cove; c) central section of the Shoesmith Glacier moraine; d, e, g, h, i, and j) granitic boulder samples and their ages; f) ages of erratic pink granite block samples (adapted from Çiner et al., 2019) indicate ice sheet retreat 9.4 ± 0.8 ka ago; k) pebbles and cobbles collected for making single amalgamated samples along with their respective ages. (For interpretation of the references to colour in this figure legend, the reader is referred to the Web version of this article.)

deposits in Marguerite Bay using Google Earth (Fig. 1c), which was later supplemented by brief field surveys in select areas. Most moraines appear fresh, with sharp ridges and little to no weathering, vegetation, or soil development. They are next to active tidewater glaciers, and are concentrated primarily in the central-eastern part of Marguerite Bay. We undertook fieldwork in the austral summer/fall of 2018 and 2022, during which we mapped the geomorphological units and collected samples from three moraine sets on three different glaciers on Horseshoe Island and Calmette Peninsula. The geomorphological map of Horseshoe Island, including the main glacial, periglacial, and coastal features, was subsequently published by Yıldırım (2020), which we also utilised in this work.

3.2. Terrestrial Cosmogenic Nuclide (TCN) surface exposure dating

3.2.1. TCN sampling strategy

The Turkish Antarctic Mission (TAE-II) was conducted in April 2018. We faced frequent interruptions due to bad weather conditions and the presence of sea ice, which limited our ability to navigate and collect samples from our target areas. Consequently, in addition to the usual sampling from boulder tops, we had to employ various sampling strategies to optimise our work.

At the Shoesmith Glacier moraine on Horseshoe Island, we encountered a situation where the traditional method of boulder surface

chipping sampling with a hammer and chisel was not feasible due to logistical and weather constraints. Instead, we selected three pink platy granite cobbles from the *ca.* 10 m^2 moraine surface, measuring *ca.* 10–15 cm in diameter and *ca.* 5–8 cm in height, and marked the upper part. Once in the laboratory, we chipped the uppermost 3–4 cm of each cobble and combined them to create a single, accurately representative amalgamated sample (HM-18-05). The same procedure was followed for three grey granite cobbles from the same moraine to obtain another amalgamated sample (HM-18-06).

Another sampling method we used on the Shoesmith Glacier moraine involved collecting 50 randomly scattered pink granite pebbles within *ca.* 10 m^2 , each *ca.* 1–3 cm in diameter, and combining them into a single amalgamated sample (HM-18-03). Similarly, we gathered 50 grey granite pebbles of comparable size to create another sample (HM-18-04). A similar amalgamation method was successfully used in our previous works (e.g., Çiner et al., 2017; Köse et al., 2022) and is detailed in Sarıkaya et al. (2017) and elsewhere (Repka et al., 1997; Wetterauer et al., 2022).

Later, during the 2022 Turkish Antarctic Expedition (TAE-VI), we also collected six additional samples from the boulder surfaces of the Shoesmith Moraine using a chisel and hammer from two separate sets. The first set comprises three samples (Cosmo 1a, 1b, 1c) located near the Lystad Bay area. The other set includes three additional samples (Cosmo 2a, 2b, 2c) from the Gaule Cove part of the moraine. In summary, we

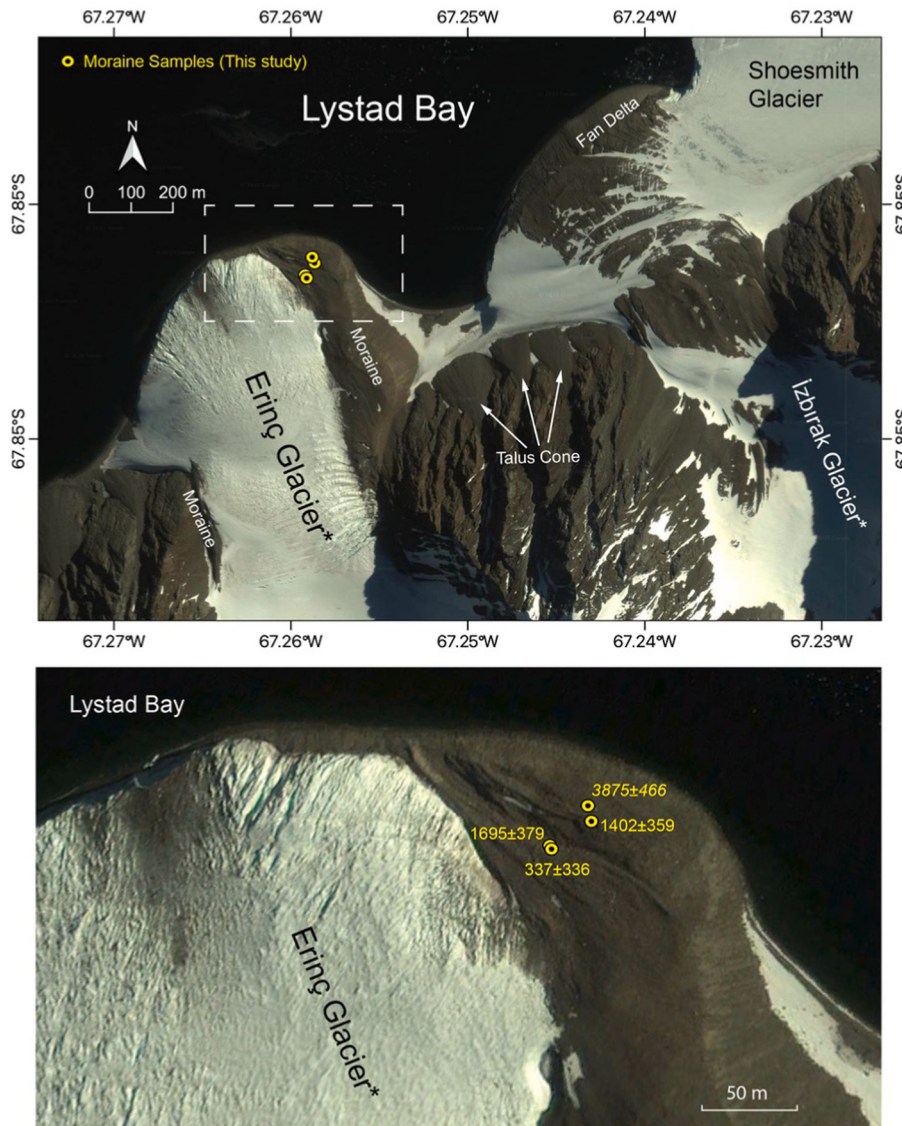


Fig. 5. Erinç Glacier and Moraine ridge samples on Google Earth image and their ^{10}Be TCN ages (in yellow, in years). See Fig. 2 for the location. * Unofficial glacier names. (For interpretation of the references to colour in this figure legend, the reader is referred to the Web version of this article.)

collected two samples from the cobbles, two from the pebbles, and six from the boulder tops of the Shoesmith Glacier moraine.

Additionally, we collected four additional boulder samples (HM-18-07, HM-18-08, HM-18-09, and HM-18-10) from Erinç Moraine (Horse-shoe Island) and three (CM-18-01, CM-18-02, and CM-18-03) from Erol Moraine (Calmette Peninsula). We used a hammer and chisel to extract rock fragments from the most prominent and uppermost boulders on the moraine crest. We packed the samples on-site and recorded their GPS locations, topographic shielding attributes, and sampled thicknesses (Table 1).

3.2.2. TCN sample preparation and analysis

The samples were prepared at three cosmogenic sample preparation laboratories: Istanbul Technical University's ITU/Kozmo-Lab (www.kozmo-lab.itu.edu.tr/en), the University of Potsdam (Germany), and Korea University's cosmogenic laboratory. Following general protocols, we crushed and sieved the rock samples to a grain size of 0.25–0.71 mm. We rinsed the crushed samples with Milli-Q water, leached them overnight in 5 % HNO_3 in an ultrasonic bath, and utilised a Frantz magnetic separator to collect non-magnetic minerals. The sample was primarily reduced to quartz and feldspar fractions, which were then separated

from the quartz by froth flotation. Following the standard protocol by [Kohl and Nishiizumi \(1992\)](#), the samples were leached using a 1:1 hydrochloric acid (HCl) solution and 1–2 % hydrofluoric acid (HF). Additional leaching was conducted using hexafluorosilicic acid (H_2SiF_6), as described by [Brown et al. \(1991\)](#), to ensure the acquisition of clean quartz. The quartz grains were dissolved in HF, and approximately 90 μl of 3.2×10^{-3} g/g ^{9}Be carrier in 1N HCl with a density of 1.010 g cm⁻³ was added. The ion-exchange column chemistry for beryllium extraction followed the procedures of [Blanckenburg \(2005\)](#). Extracted beryllium hydroxide (Be(OH)_2) was oxidised, and niobium (Nb) powder was added in mixing ratios of 4:1. All Accelerator Mass Spectrometry analysis of ^{10}Be was performed at the Korea Institute of Science and Technology in Seoul ([Kim et al., 2024](#)).

Ages were calculated using version 3 of the CRONUS-Earth Online Calculator on May 31, 2024 (<https://hess.ess.washington.edu>) ([Balco et al., 2008](#)). We employed the Lifton/Sato flux time-dependent scaling scheme (known as LSDn or SF) based on [Lifton et al. \(2014\)](#). Corrections for sample thickness and topographic shielding were applied. Sample densities were assumed to be 2.65 g/cm³. Bedrock erosion rates following deposition were ignored, consistent with other research in most Antarctic samples. We used “error-weighted mean age” to calculate

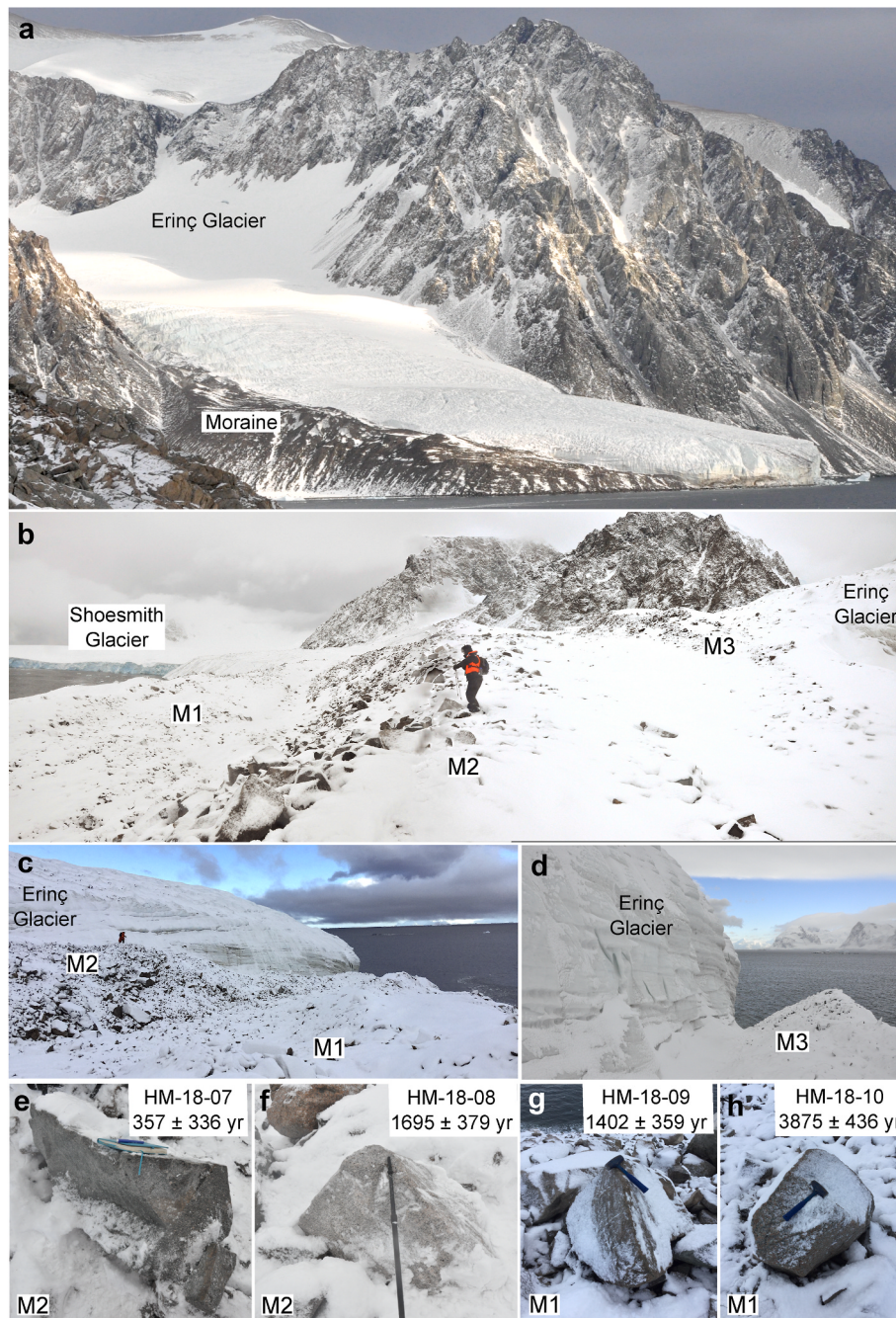


Fig. 6. a) General view of the Erinç Glacier, featuring the right lateral moraine calving into Lystad Bay; b) recessional moraine ridges (M1, M2, M3); c) samples from recessional ridges, M1 and M2; d) the Erinç Glacier alongside the undated youngest recessional ridge (M3); e-h) samples and their respective ages.

the landform ages after excluding the outliers. All essential information needed to reproduce the sample ages is provided in [Supplementary Table 1](#).

4. Results

4.1. Shoesmith Moraine

As previously mentioned, we gathered ten samples from the Shoesmith Moraine. The two amalgamated samples, HM-18-03 and HM-18-04, yielded ages of 4619 ± 491 years and 4864 ± 503 years, respectively. Additionally, the two samples, HM-18-05 and HM-18-06, composed of three cobbles mixed into a single amalgamated sample, yielded ages of 832 ± 321 years and 366 ± 364 years, respectively

([Table 1](#); [Figs. 3 and 4](#)).

Apart from Cosmo 1a, the other five boulder samples have closely matching results. Cosmo 1a, 1b, and 1c yielded ages of 1347 ± 509 years, 617 ± 487 years, and 315 ± 359 years, respectively. The other samples, Cosmo 2a and 2c, yielded ages of 528 ± 376 years and 473 ± 424 years, respectively ([Table 1](#); [Figs. 3 and 4](#)).

4.2. Erinç Moraine

We collected two samples from each of the prominent moraine ridges (M2 and M3) of the Erinç Moraine. The samples HM-18-07 and HM-18-08 from moraine M2 yielded ages of 357 ± 336 years and 1695 ± 379 years, respectively. Samples HM-18-09 and HM-18-10 from moraine M3 gave ages of 1402 ± 359 years and 3875 ± 466 years, respectively

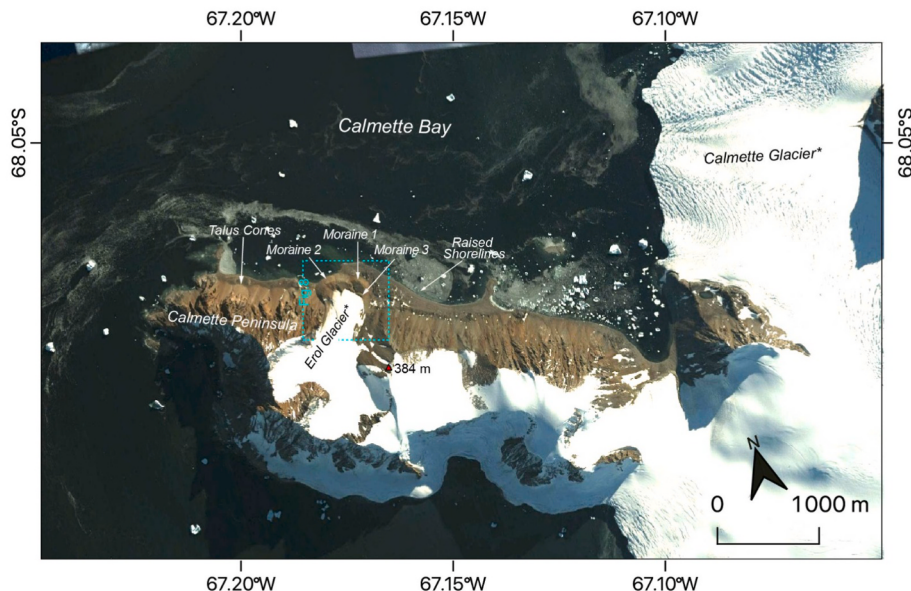


Fig. 7. Calmette Peninsula main geomorphic features on Google Earth image. Fig. 8 location is shown in a blue box. (For interpretation of the references to colour in this figure legend, the reader is referred to the Web version of this article.)

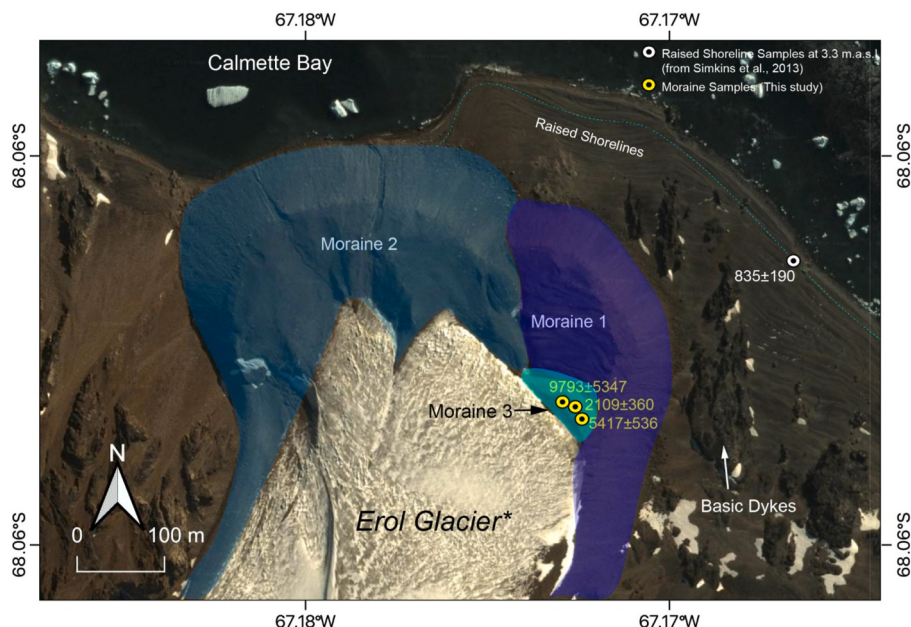


Fig. 8. a) Google Earth image of the Erol Glacier and its moraines (M1, M2, and M3) along with the ^{10}Be TCN ages of the boulder samples from the youngest moraine (M3). * Unofficial glacier name. M2 overlies the raised shoreline at 3.3 m asl, OSL-dated to 835 ± 190 years by Simkins et al. (2013).

(Table 1; Figs. 5 and 6).

4.3. Erol Moraine

The three samples collected from Erol Moraine are located only a few metres apart but have distinct ages. The samples CM-18-01, CM-18-02, and CM-18-03 yielded ages of 5417 ± 536 years, 2109 ± 360 years, and 9793 ± 850 years, respectively (Table 1; Figs. 8 and 9).

5. Discussion

5.1. ^{10}Be chronology of Marguerite Bay moraines

We mapped several areas along Marguerite Bay where probable Neoglacial moraines are present (Fig. 1c). Below, we discuss the ones we dated using ^{10}Be TCN.

5.1.1. Shoesmith Moraine

As explained above, we collected three different sample types from the Shoesmith Moraine. Only one sample (Cosmo 1a = 1347 ± 509 years) is considered an outlier due to a likely inherited ^{10}Be inventory among the five dated granitic boulders. It has greater uncertainty, as it



Fig. 9. a) General view of the Erol Glacier and end moraines from the oldest (M1) to the youngest (M3); b) M3 boulder samples and ages; c and f) M3 moraine details at the contact with the Erol Glacier; d) oldest moraine (M1) and the beach ridges; e) M3 sampled boulder and its age.

spreads more than other closely clustered samples on the same moraine (Fig. 10, Table 1).

The amalgamated cobble samples (HM-18-05 and HM-18-06) yielded ages of 832 ± 321 years and 366 ± 364 years, respectively. On the other hand, the amalgamated pebble samples (HM-18-03 and HM-18-04) are internally consistent (4619 ± 491 years and 4864 ± 503 years, respectively) but yielded unexpectedly high ages compared to the remaining samples. This may be related to all pebbles being fragmented from high-inheritance-bearing boulders during transport. It may also be due to the smaller-sized samples, which may retain a selectively higher concentration of inherited nuclides. We are unable to explain these old ages adequately. In any case, collecting pebble samples proved ineffective in this environment and should be omitted as a sampling method.

We also note that one cobble (HM-18-06) and some of the boulder samples (Cosmo1b, 1c, 2a, and 2c) are very close to the background limits and have total Be inventories that are less than twice the measured

blank. Although we acknowledge this condition, we still used these ages, as they indicate that they are very young, which aligns with other ages obtained in the area. Consequently, we disregarded two pebble samples and one boulder sample from our calculations. Therefore, the error-weighted mean landform age for the Shoesmith lateral moraine is calculated to be 496 ± 79 years. This age marks the end of the Neoglacial period and represents the formation of the Shoesmith Moraine during the LIA. Including the boulder sample in the calculations would result in a landform age of 648 ± 148 years, which does not significantly alter our interpretation.

5.1.2. Erinç Moraine

The right lateral moraine of the Erinç Glacier consists of numerous recessional ridges. The samples collected from the two ridges showed a scattered age range, complicating interpretation. Recognising that polygenetic moraine formation can occur due to various glacial advances,

Table 1

Sample locations, types, and local corrections to production rates. ^{10}Be TCN ages of samples and the error-weighted mean age for each landform are also marked.

Sample ID	Location and Moraine	Sample type	Latitude	Longitude	Elevation	Thickness	Topo shielding	Exposure age	1σ error ^{Int}	1σ error ^{Ext}	Error-weighted mean landform age
			(WGS 84)	(WGS 84)	(a.s.l.)	(cm)	(–)	(yr)	(yr)	(yr)	(yr)
			(S)	(W)	(m)						
HM-18-03	Horseshoe Shoesmith Moraine	Pebbles	-67.83360	-67.22240	70	1	0.99768	* 4619	327	491	496 ± 79
HM-18-04	Horseshoe Shoesmith Moraine	Pebbles	-67.83370	-67.22310	81	1	0.99768	* 4864	323	503	
HM-18-05	Horseshoe Shoesmith Moraine	Cobbles	-67.83420	-67.22480	87	5	0.99768	832	315	321	
HM-18-06	Horseshoe Shoesmith Moraine	Cobbles	-67.83420	-67.22480	87	5	0.99768	366	363	364	
Cosmo 1a	Horseshoe Shoesmith Moraine	Boulder	-67.83456	-67.23158	64	3	0.99768	* 1347	498	509	
Cosmo 1b	Horseshoe Shoesmith Moraine	Boulder	-67.83445	-67.23059	69	3	0.99768	617	485	487	
Cosmo 1c	Horseshoe Shoesmith Moraine	Boulder	-67.83439	-67.22950	74	3	0.99768	315	358	359	
Cosmo 2a	Horseshoe Shoesmith Moraine	Boulder	-67.83192	-67.21932	83	3	0.99768	528	373	376	
Cosmo 2c	Horseshoe Shoesmith Moraine	Boulder	-67.83204	-67.21980	82	3	0.99768	337	423	424	
HM-18-07	Horseshoe Erinç M2 Moraine	Boulder	-67.85140	-67.25930	27	3	0.98276	357	335	336	1178 ± 402
HM-18-08	Horseshoe Erinç M2 Moraine	Boulder	-67.85140	-67.25930	24	4	0.98461	1695	355	379	
HM-18-09	Horseshoe Erinç M1 Moraine	Boulder	-67.85120	-67.25890	20	3	0.98383	1402	341	359	
HM-18-10	Horseshoe Erinç M1 Moraine	Boulder	-67.85110	-67.25900	20	3	0.98383	* 3875	351	466	
CM-18-01	Calmette Erol M3 Moraine	Boulder	-68.06260	-67.17240	84	3	0.99021	* 5417	323	536	all outliers
CM-18-02	Calmette Erol M3 Moraine	Boulder	-68.06260	-67.17240	84	5	0.99021	* 2109	319	360	
CM-18-03	Calmette Erol M3 Moraine	Boulder	-68.06260	-67.17240	84	3	0.99021	* 9793	347	850	

Notes: All exposure ages were computed assuming zero erosion and a rock density of 2.65 g cm^{-3} , using the online exposure age calculator (v3, wrapper 3.0.2, const 2024-08-26) of [Balco et al. \(2008\)](#) with the “St” scaling scheme and the implemented production rate calibration dataset. Both internal uncertainties (including measurement uncertainties) and external uncertainties (including only production rate uncertainties) are presented. Landform ages were calculated via error-weighted averaging using external uncertainties of all samples that belong to the specific landforms. All ancillary information about samples can be found in the supplementary table. *Outliers are in italic and denoted by **.

we present several alternative interpretations and highlight our preferred scenario below.

- The first scenario treats both recessional ridges as a single moraine and calculates the average of all four samples, yielding the error-weighted mean landform age as 1994 ± 771 years. However, because there are two distinct and clearly laterally continuous geomorphic ridges, we exclude this scenario from further consideration.
- In the second scenario, we exclude the ages of the youngest and oldest boulders from the calculations. The oldest sample (HM-18-10 = 3875 ± 466 years) from the external ridge (M1) is considered an outlier, as its age is significantly higher than that of the other samples, likely due to high inheritance. The internal ridge’s (M2) youngest sample (HM-18-07 = 357 ± 336 years) is also much younger than the other ages, likely due to overturning. Treating

these two samples as outliers and averaging the two remaining samples would yield the error-weighted mean landform age as 1552 ± 147 years.

- A third scenario would consider the youngest (from M2) and oldest (from M1) samples as outliers and assign the age of each boulder to its respective recessional ridge, resulting in M1: HM-18-08 = 1402 ± 359 years and M2: HM-18-09 = 1695 ± 379 years. This outcome indicates that the external moraines are younger than the internal ones, which lack morphostratigraphic significance. Therefore, this scenario was also rejected.
- A fourth scenario would determine the landform age using either the youngest (357 ± 336 years) or the oldest (3875 ± 466 years) obtained age. The oldest age seems unlikely due to the fresh appearance of the moraine, suggesting a possible problem with the inheritance of the boulder. On the other hand, the youngest age obtained from a boulder on the M2 ridge might actually represent the true age of the

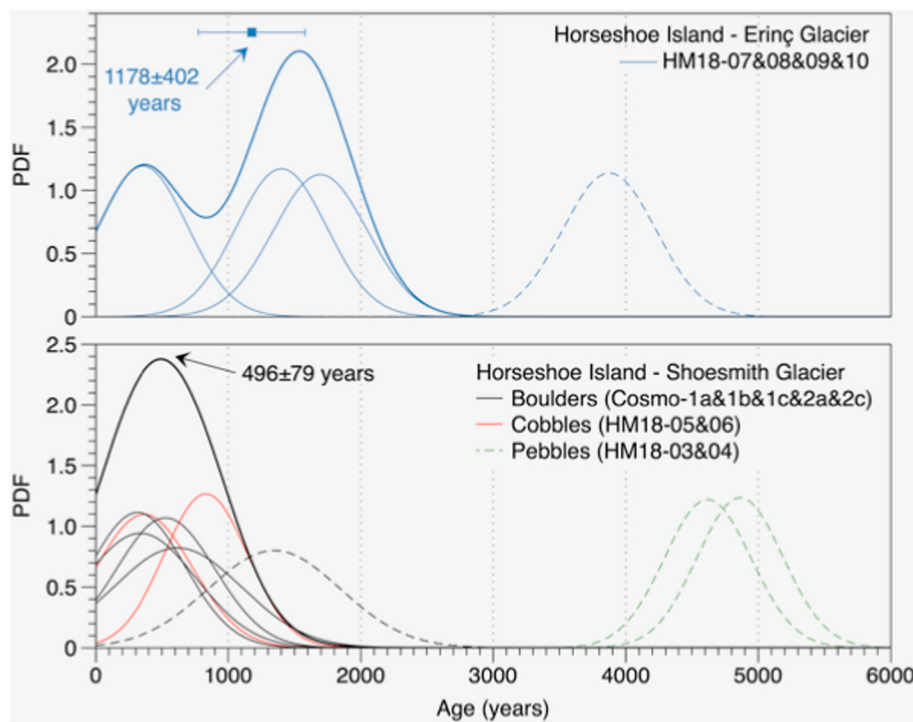


Fig. 10. Sample ages and their Probability Density Function (PDF). Dashed lines indicate outlier samples.

moraine. However, this possibility is ruled out as there is another ridge closer to the glacier.

- A fifth scenario suggests that the moraine ridges are the result of various glacial stillstands (polygenic moraines), which explain the scattered age distribution. This scenario is also excluded as the boulder ages are inconsistent within each ridge.
- In the sixth and final scenario, only the oldest boulder age ($\text{HM-18-10} = 3875 \pm 466$ years) from M1 is considered an outlier. In this case, the error-weighted mean landform age for the Erinç Moraine is calculated to be 1163 ± 403 years.

Among the proposed scenarios, we favour the final scenario and suggest a formation age of 1163 ± 403 years for the Erinç Moraine, corresponding to the late Neoglacial period. Although we have opted to use the value from our final scenario, choosing the average ages from all other scenarios would yield similar average ages, ranging from 1552 ± 147 years to 1994 ± 771 years. Regardless of the scenarios selected, the ages indicate that the Erinç Moraine was formed during the late Neoglacial period. Given the significant uncertainties in the error margins, a LIA could be tentatively attributed to the undated moraine ridge (M3), located just a few tens of metres from the actual glacier front.

5.1.3. Erol Moraine

The ages of the three boulders from the Erol Moraine exhibit a wide scatter, ranging from ca. 2 to 10 ka (Table 1). To determine the age of a moraine from boulders, it is common practice to calculate the error-weighted mean age while excluding outliers (e.g., Applegate et al., 2012). However, several processes, including a polygenic origin, may result in a significant scatter of observed boulder ages, rendering the mean age approach obsolete. To address this issue, some researchers propose using the oldest boulder age to represent the landform's age, as the widespread ages of boulders are formed through the erosion of moraine surfaces and the exhumation of uneroded fresh boulders (e.g., Putkonen and Swanson, 2003). As a result, the authors suggest that in fresh-looking landforms, the maximum age of the oldest boulder is likely to be 90 % of the moraine's age, with a 95 % probability. Additionally, they indicated that only 3 % of all moraine boulders in their

comprehensive dataset had previously been exposed (Putkonen and Swanson, 2003). Although significantly more TCN surface exposure data are now accessible, this interpretation has so far remained uncontested.

Utilising a comprehensive dataset from the Tibetan Plateau, Heyman et al. (2011) demonstrated that the incomplete exposure (post-depositional shielding) model is significantly more effective than the prior exposure (inheritance) model. Consequently, the authors suggested that for boulder groups with varying exposure ages, the oldest apparent exposure age should typically be considered a minimum deglaciation age unless there are independent signs of previous exposure.

In Antarctica, several studies have highlighted the significant challenges of TCN exposure dating using moraine boulders and deglaciated bedrock, which can yield anomalously old ages (e.g., Fernández-Fernández et al., 2021). These studies indicate the presence of inherited cosmogenic nuclides on rock surfaces associated with the retreat of cold- and polythermal-based glaciers, resulting in complex glacial exposure histories. This underscores the importance of conducting meticulous geomorphological observations before sampling to identify and avoid potentially inherited surfaces. Additionally, in areas influenced by cold-based ice, as is the case with Erol Moraine, a multi-nuclide approach is recommended to better understand the glacial history (Hein et al., 2014).

In the case of the Erol Moraine, as the samples are only a few tens of metres from the active glacier front, they are likely to have young ages. Therefore, we decided to classify all three boulders from the Erol Moraine as outliers due to their unusually old and varied ages. We interpret this peculiar set of old ages as indicative of significant inheritance. The Erol Glacier is relatively small and has a limited source area, suggesting that the bedrock fragments incorporated into the glacier likely had high pre-exposure to cosmic radiation and were transported over short distances. The boulders may have been transported on the glacier surface and/or through limited subglacial erosion, which explains the issue of inheritance.

A recent study by Swanger et al. (2024) in a cirque moraine of the Western Olympus Range in the McMurdo Dry Valleys demonstrated the significance of slow bedrock erosion rates in producing exposure age

scatter. The authors reported significantly higher concentrations of inherited nuclides in dolerites compared to sandstones, emphasising the importance of hard lithologies in resisting erosion. This pattern also applies to the warmer regions of the Antarctic Peninsula, as evidenced by the polythermal ice caps of the Hurd Peninsula and the South Shetland Islands. Fernández-Fernández et al. (2021) demonstrated that nuclide inheritance complicates the interpretation of TCN ages due to limited subglacial erosion beneath cold-based ice, often resulting in anomalously old exposure dates. This challenge could be addressed by using an *in situ* ^{14}C and ^{10}Be pair in future studies. In the absence of independent chronological constraints, it is challenging to quantify the inherited nuclide signal and accurately reconstruct the timing of deglaciation. This assumption should also apply to the overestimated boulder ages of Erol Moraine.

Although ^{10}Be TCN dating of moraine boulders has proven ineffective in determining the actual formation age of the Erol Moraine, a well-constrained stratigraphic cross-cutting relationship provides clarity. Numerous raised beach ridges have been identified along the Calmette Peninsula shoreline (Bentley et al., 2005b; Hodgson et al., 2013; Simkins et al., 2013; Simms et al., 2021; Yıldırım et al., 2024). Simkins et al. (2013) OSL-dated a beach ridge at 3.3 m asl (their beach 3 level) to 835 ± 190 years BP. Since several younger beach ridges than beach 3 of Simkins et al. (2013) exist further west and are overrun by the second Erol Moraine (M2), this glacial advance must have taken place after 835 ± 190 years BP (Fig. 9d).

Therefore, the M3 moraine, which is the closest to the glacier front (ca. 25 m) that we attempted to date, should be even younger. This suggests a glacial advance during the LIA, as previously proposed for the entire moraine complex (Simkins et al., 2013; Simms et al., 2021). Future TCN dating efforts should focus on the three end moraines and the well-preserved left lateral moraine of the Erol Glacier to enhance understanding of the timing and potential causes of inheritance in the boulders. Alternative methods, such as ^{14}C and OSL, could help solve the age issue in these challenging settings, provided suitable material is available.

5.2. The timing of the recent glacial advance in Marguerite Bay

Our age data from both Horseshoe Island and Calmette Bay indicate that the most recent glacial advance in the Marguerite Bay area occurred during the late Neoglacial period, particularly during the LIA. This period is documented by the numerous recessional ridges, which can be up to 200 m wide in their largest extent, on the Erinc Moraine on Horseshoe Island. Considering that the average age of the two recessional ridges closer to the glacier yielded 1163 ± 403 years, one could assume that older external ridges represent the onset of the late Neoglacial period in that area. On the other hand, the undated recessional moraine ridge, which is closest to the active glacier, could tentatively be attributed to the LIA. Dating the outermost and innermost ridges in the future would enhance the chronology of this moraine.

The Shoesmith Moraine has been dated to 496 ± 79 years and represents the culmination of the LIA. This advance is further confirmed at the Calmette Peninsula, located just 20 km to the south, where the Erol Moraine's second end lobe (M2) overrides the OSL-dated (835 ± 190 years) beaches at 3.3 m asl (Simkins et al., 2013). In conclusion, it is now clear that LIA advances, primarily associated with the Northern Hemisphere, have also taken place in the Antarctic Peninsula, as previously noted by several studies (e.g., John and Sudgen, 1971; Porter, 2001; Ingólfsson et al., 2003; Palacios et al., 2020; Simms et al., 2012, 2021; Oliva et al., 2024). In the following section, we will briefly discuss the proxies related to the Neoglacial period, including the LIA, in the Western Antarctic Peninsula.

5.3. Neoglacial period in the western Antarctic Peninsula

Various proxy data indicate the advance of glaciers at the onset of the

Neoglacial period, ca. 4000 years ago, in the Antarctic Peninsula. As glacier advances during the Neoglacial period are now being better constrained, an increasing number of sites indicate LIA cooling (e.g., Clapperton and Sugden, 1988; Ingólfsson et al., 1998; Palacios et al., 2020; Simms et al., 2021) (Fig. 11).

A recent study by Palacios et al. (2020) provides a comprehensive review of landform formations from the Neoglacial period in the Antarctic Peninsula, with a focus on the South Shetland Islands. The authors concluded that the primary Neoglacial advances were mostly synchronous, coinciding with cold periods, as is the case with other proxies such as glacio-isostatic marine terraces, marine, and lacustrine sediments.

Additionally, by incorporating available timing constraints into a Bayesian model, Simms et al. (2021) estimated an age of 400 to 90 cal years BP (1550–1860 CE; 95 %) for the LIA across the Antarctic Peninsula. According to this Bayesian framework, a two-phase glacial advance fits Antarctic Peninsula data better, indicating advances from 575 to 330 cal. BP (1375–1620 CE) and from 400 to 50 cal. BP (1550–1900 CE). However, the authors suggest that further research is needed to determine whether such a two-phase advance actually occurred.

To avoid repetition, after summarising the available proxies related to the Western Antarctic Peninsula and the Southern Shetland Islands, we focus on new Neoglacial evidence, including the LIA, published since the papers by Palacios et al. (2020) and Simms et al. (2021).

5.3.1. Glacial deposits

Our study presents the first-ever ^{10}Be TCN surface exposure moraine ages from the late Neoglacial period, specifically during the LIA, in the Marguerite Bay area. In the central part of Blind Bay, ca. 40 km northeast of Horseshoe Island, submarine transverse, crescent-shaped, and longitudinal ridges resembling undisturbed moraines, located just a few kilometres from the modern ice front, were interpreted as evidence of grounded ice stabilisation during the LIA (Garcia et al., 2016). A series of smaller landforms exhibiting alternating minor readvances was also observed in this fjord. Similar elongated features were also observable just a few hundred meters from the Shoesmith Glacier, likely representing the continuation of the Shoesmith Moraine beneath the sea (Tükenmez et al., 2022).

In the southernmost part of the Western Antarctic Peninsula, early Neoglacial advances were reported on the highest lateral moraine on Alexander Island, at 4.4 ± 0.7 and 1 ka (^{10}Be TCN ages) (Davies et al., 2017). The remaining TCN data on the Neoglacial period originate from the Southern Shetland Islands, ca. 120 km off the Northwestern Antarctic Peninsula. A recent study by Oliva et al. (2024) reported numerous small glacier advances and retreats on Livingston Island since the onset of the Neoglacial period. At the BAE Glacier in the Hurd Peninsula, informally known as the Spanish Base Valley lobe, moraine ridges have yielded ages ranging from 4.9 to 1.4 ka ago, with the most recent age being closest to the current glacier front.

Oliva et al. (2024) also dated several LIA advances of the BAE Glacier using ^{10}Be TCN. These advances were more limited than earlier Neoglacial advances and reached their maximum extent in the 17th century. A whalebone discovered atop a moraine ridge on Livingston Island dates the glacial advance to ca. 1690 CE (Björck et al., 1996). This age is comparable to the advances of the Shoesmith and Erol glaciers in the Marguerite Bay area. In contrast, Palacios et al. (2020) found no evidence of LIA moraines on the Byers Peninsula, located at the westernmost fringe of Livingston Island. Here, the central plateau was deglaciated at 7–8 ka (Oliva et al., 2016), and Neoglacial advances occurred at 4.1 ± 0.5 and 1.0 ± 0.2 ka (Palacios et al., 2020).

On the northern plateau of the Fildes Peninsula on King George Island, the largest island in the Southern Shetland Islands, ^{36}Cl TCN ages obtained from polygenic moraines indicate two Neoglacial advances occurring ca. 4.6 and 1.0 ka (Oliva et al., 2023). On the Fildes Peninsula, the most significant LIA glacier advance took place around the 14th century (Hall, 2007; Heredia-Barion et al., 2023a).



Fig. 11. Proxy data related to the LIA advance in the Western Antarctic Peninsula (WAP) and South Shetland Islands (SSI). MB: Marguerite Bay, KGI: King George Island, LI: Livingston Island, MIS: Müller Ice Shelf. Modified from Palacios et al. (2020) [Barnard et al., 2014; Birkenmajer, 1981; Christ et al., 2015; Curl, 1980; Hall, 2010; John and Sugden, 1971; Khim et al., 2002; Reilly et al., 2016; Shevenell et al., 1996].

5.3.2. Lacustrine and bio-sedimentary archives

Unlike moraines, which indicate stabilisation in glacial retreats, sedimentary and especially lacustrine sequences often provide continuous, high-resolution records of past events. However, while the Eastern Antarctic Peninsula is relatively better exploited (e.g., Čejka et al., 2020; Roman et al., 2024), the lacustrine records of the Western Antarctic Peninsula represent an underexplored resource for understanding Neoglacial climate and environmental changes (Giralt et al., 2020).

For instance, diatom data from a core taken at Skua Lake on Horseshoe Island indicate a rapid transition from a marine to a freshwater environment, resulting in the isolation of the basin after 1860 cal years BP (Wassell and Håkansson, 1992). In Marguerite Bay, Hodgson et al. (2013) interpreted the decline in organic carbonate content and sediment accumulation rates from 2630 to 2030 cal years BP at Narrows Lake (Pourquoi Pas Island, located 15 km north of Horseshoe Island) and Col Lake 1 (Horseshoe Island), respectively, as an indicator of the onset of Neoglacial expansion. This age is comparable to the late Neoglacial development of the Erinç Moraine.

The authors also note that this coincides with an increase in smaller sub-angular clasts on the raised beaches of Horseshoe Island after ca.

2400 ^{14}C years BP. This aligns with the cooler conditions observed in Neny Fjord, 40 km south of Horseshoe Island, where a sand-rich interval and associated reduction in biogenic sediment content between ca. 2800 and 2500 cal years BP were encountered in a marine core ca. 5 km from land. This suggests a modest glacier advance when the glacier front was sufficiently close to transport coarse-grained materials to the core location (Allen et al., 2010).

However, in contrast to our findings from the Erinç and Shoesmith moraines, Hodgson et al. (2013) reported no evidence of cooling between 1150 and 400–410 cal years BP. The authors interpret the increase in *Gomphonema* species (diatom) and organic carbon in the uppermost part of the Narrows Lake (Pourquoi Pas Island) core after ca. 410 cal years BP, along with the increased sedimentation rates in the Col Lake 1 (Horseshoe Island) core after ca. 400 cal years BP as a response to late Holocene warming. This discrepancy between the Col Lake 1 and Shoesmith Moraine records from two sites just a few hundred meters apart underscores the complex interplay between temperature and precipitation patterns at both annual and seasonal scales that shape regional ecosystem dynamics. Further research should shed light on the coupling between past climate and glacier response in the region.

At Rothera Point, near the British Antarctic Survey's Rothera Research Station, Guglielmin et al. (2016) ^{14}C dated moss and the underlying soil at the southern limit of the Wormald Ice Piedmont. They reported that a period of glacial advance began between 671 and 558 cal years BP ago, continuing at least until 490–317 cal years BP. This glacial advance is comparable to the Shoesmith Glacier's LIA advance, which we dated to 496 ± 79 years, located less than 50 km southeast of Rothera Point, emphasising the significance of local effects.

In the Anvers and Galindez Islands along the Western Antarctic Peninsula, Yu et al. (2016) determined that the interval from 900 to 600 cal years BP was the coldest. This was evidenced by ice expansion, the high number of kill ages from mosses recently uncovered by retreating glaciers, and a noticeable gap in the formation of peat banks.

In the South Shetland Islands, ^{14}C ages from mosses embedded in glacial deposits on the Potter Peninsula (King George Island), near the glacier front, suggest that a Neoglacial advance took place between 1.7 and 1.4 cal ka BP (Heredia-Barión et al., 2023b). Additionally, geomorphic and ^{210}Pb varve dating evidence indicate a glacial readvance most likely occurring between 0.5 and 0.1 cal ka BP during the LIA (Heredia-Barión et al., 2023b). Furthermore, a geochemical study of ornithogenic sediments shows a decline in penguin populations on Ardley Island between 450 and 200 cal years BP (Liu et al., 2005).

Moreover, multi-proxy data from lakes and mosses on moraines of the Fildes Peninsula on King George Island suggest four-stage glacial advances between ca. 5.3 and 0.7 cal ka BP (Heredia-Barión et al., 2023a). Furthermore, the analysis of a 1.5 m-thick sediment core from Midge Lake, Byers Peninsula, Livingston Island, revealed several peaks in sediment, algae, pollen, spores, and diatom assemblage changes between 3.2 and 2.7 ka BP (Björck et al., 1991). This suggests a correlation between rising humidity and glacier expansion.

5.3.3. Other proxies

Several additional proxies, such as marine records, ice cores, and raised beaches, further enhance our understanding of the Neoglacial period, particularly during the LIA. For instance, the sea ice and cooler sea-surface and bottom water conditions observed in Palmer Deep, located off the central Western Antarctic Peninsula, from 700 to 150 cal years BP were linked to multiple glacial advances (e.g., Domack et al., 2001; Taylor and Sjunneskog, 2002; Warner and Domack, 2002).

Global circulation models simulating surface mass balance (snow accumulation) over the past millennium indicate that snowfall in West Antarctica reached its lowest levels during the LIA (Dalaïden et al., 2020). Nevertheless, during the LIA, ice shelves, including Rotch Dome on Livingston Island (Björck et al., 1996) and the Müller Ice Shelf (Domack et al., 1995), are known to have expanded. Furthermore, a geochemical study of ornithogenic sediments indicates a decline in penguin populations on Ardley Island, South Shetland Islands, between 450 and 200 cal years BP (Liu et al., 2005).

Ice-rafter detritus received along the raised beaches was also used as a proxy for climate. On Livingston Island, although the modern beach contains little local debris, raised beaches, ^{14}C dated to ca. 250 and 1750 cal. BP comprises substantial quantities, including debris derived from the Antarctic Peninsula (Hall and Perry, 2004). The authors interpret this rise in ice-rafter detritus as indicative of increased glacial activity, alterations in ocean circulation, and/or better preservation of icebergs.

Certain coastal ecosystems, notably those of marine invertebrates along the Antarctic Peninsula, have undergone niche restructuring in response to Neoglacial sea-level fluctuations. For example, genetic studies on Antarctic gastropod limpets *Nacella concinna* reveal that population bottlenecks occurred during cooler periods with lower sea levels (1.8–1.2 ka), followed by rapid expansion into newly submerged areas (Suda et al., 2015).

5.3.4. Final remarks and outlook

Evidence suggests that the main late Neoglacial advances,

particularly during the LIA, in the Western Antarctic Peninsula occurred essentially simultaneously, despite some local variations. These glacial advances occurred during periods of cooler temperatures, as indicated by various proxy data sources, including TCN and ^{14}C age data from moraines, along with information from marine and lake settings, respectively (Palacios et al., 2020).

Dating of glacial landforms using TCN methods is starting to increase our understanding of glacier behaviour since the onset of the Neoglacial, but the available data remain scarce. Future research should focus on more fresh-looking moraines near land-terminating and tidewater glaciers, as well as lake sediments in ice-free coastal areas, particularly those adjacent to moraines, which could help bridge this knowledge gap and refine regional climate models. The Marguerite Bay area stands out as an excellent candidate, as several undated moraines (Fig. 1c) and lakes are awaiting exploration.

In any case, the proximity of the internal moraine ridges formed during the LIA to the present glacier fronts (ca. 25–50 m) suggests remarkable stability of the regional ice masses, despite the pronounced warming recorded in recent decades (Turner et al., 2014). Future research should investigate how this apparent stability may be affected in the context of continued warming projected for the Antarctic Peninsula in the coming decades, particularly when combined with anticipated increases in precipitation (IPCC et al., 2019).

6. Conclusions

The Neoglacial record (ca. 4 to 0.2 ka ago), including the Little Ice Age (ca. between 1300 and 1850 CE) on the Western Antarctic Peninsula, which is mainly represented by moraines and lake sediments, remains poorly constrained. In this study, we present a non-exhaustive list of potentially datable, fresh-looking, and well-preserved moraines located next to active glaciers along Marguerite Bay, the largest bay in the Western Antarctic Peninsula. By utilising ^{10}Be Terrestrial Cosmogenic Nuclide (TCN) surface exposure dating, we refined the timing of late Neoglacial glacier fluctuations, concentrating on three moraines from three different glaciers.

Due to adverse weather conditions, time constraints, and logistical challenges, we had to employ various sampling strategies to optimise our work. Subsequently, in addition to typical boulder top sampling, we also utilised easily collectable sets of pebbles (50 pebbles) and cobbles (3 cobbles). Our results demonstrate that collecting three cobbles from the moraine surface and combining them to create a single, accurately representative amalgamated sample is an efficient and time-saving method that could be particularly useful, especially in Antarctica, where well-polished surfaces are difficult to break. However, this method requires further testing to gain universal acceptance. Conversely, collecting pebble samples and merging them to form a single amalgamated sample resulted in internally consistent but unreasonably high ages (ca. 5 ka). This method is not a viable solution and should be avoided.

Results obtained from pebbles, cobbles, and boulder samples ($n = 9$) indicate that the Shoesmith Moraine on Horseshoe Island stabilised during the LIA at 496 ± 79 years, marking the end of the Neoglacial period.

The boulders ($n = 4$) from the Erinç Moraine on the same island record earlier late Neoglacial advances between 1552 ± 147 years and 1994 ± 771 years, depending on the chosen scenario. We prefer to regard the oldest boulder age as an outlier and report the error-weighted mean landform age of 1163 ± 403 years. Regardless of the selected scenarios, the ages indicate that the Erinç Moraine was formed during the late Neoglacial period. Because of substantial uncertainties in the error margins, a tentative connection to a LIA may be made with the undated and stratigraphically youngest moraine ridge, located just a few tens of meters from the current glacier front.

Three closely spaced boulder samples ($n = 3$) from the Erol Moraine (Calmette Peninsula), located only a few tens of metres from the active

glacier front, yielded anomalously high ages (*ca.* 2, 5 and 10 ka) due to inherited nuclides that were not zeroed, likely because of limited subglacial erosion, supraglacial transport, and/or a short distance from the source area. However, this moraine has already been constrained to the LIA through cross-cutting relationships with previously dated raised beaches. These findings highlight the challenges in interpreting exposure ages from low-erosion glaciers while providing improved constraints on late Neoglacial and, in particular, LIA moraine formation in the Western Antarctic Peninsula. The closeness of most LIA moraines, just a few tens of meters from the current glacier fronts, suggests that the ice masses have remained relatively stable despite recent warming trends.

Future studies should focus on dating these fresh-looking moraines, characterized by sharp ridges and minimal weathering, located near active glaciers and lake sediments in ice-free coastal regions, to enhance regional climate models for the Neoglacial period. The Marguerite Bay region appears particularly promising because of its numerous undated moraines and lakes.

Declaration of generative AI and AI-assisted technologies in the manuscript preparation process:

During the preparation of this work, the authors used www.grammarly.com in order to edit the English. After using this tool, the authors reviewed and edited the content as needed and take full responsibility for the content of the published article.

Author contributions

All authors have made substantial contributions to the submission outlined below:

Attila Çiner: Founding, study design, fieldwork, sampling, writing, reading.

Cengiz Yıldırım: Founding, study design, fieldwork, sampling, writing, reading.

M. Akif Sarıkaya: Cosmogenic sample preparation, writing, reading.

Yohanna KLANLEN: Fieldwork, sampling, reading.

Marc OLIVA: Study design, writing, reading.

Yeong BAE SEONG: Cosmogenic sample preparation, reading.

Byung Yong YU: Cosmogenic sample measurements.

Declaration of competing interest

The authors declare they have no known competing financial interests or personal relationships that could influence the work reported in this paper.

Acknowledgements

This study was conducted under the auspices of the Presidency of the Turkish Republic, with support from the Ministry of Science, Industry, and Technology, coordinated by the Istanbul Technical University (ITU) Research Fund (Grant No: 10), the ITU Polar Research Center (PolReC), and the Turkish Academy of Sciences. Authors Attila Çiner and Cengiz Yıldırım carried out fieldwork in 2018, while Yolanda Klanten conducted fieldwork in 2022, funded by the Polar Portuguese Program (Project NUNANTAR, Principal Investigator: Marc Oliva). This research article has also been supported by the ANTALP research group (Antarctic, Arctic, Alpine Environments; 2021-SGR-00269), funded by the Government of Catalonia, and complements the study topics of GRELARCTIC (PID2023-146730NB-C31) and ISLANDSINTHEICE (CNS2023-144040), both funded by the Spanish Ministry of Economy and Competitiveness. We thank Prof Bodo Bookhagen from the University of Potsdam for preparing five TCN samples from the Shoesmith Moraine. We also thank the two anonymous reviewers and editor Bethan Davies for their insightful and constructive comments, which greatly

enhanced the quality of this paper.

Appendix A. Supplementary data

Supplementary data to this article can be found online at <https://doi.org/10.1016/j.quascirev.2025.109641>.

Data availability

All data and/or code is contained within the submission.

References

- Allen, C.S., Oakes-Fretwell, L., Anderson, J.B., Hodgson, D.A., 2010. A record of Holocene glacial and oceanographic variability in Neny fjord, Antarctic Peninsula. *Holocene* 20, 551–564.
- Anderson, J.B., Oakes-Fretwell, L., 2008. Geomorphology of the onset area of a palaeo-ice stream, Marguerite Bay, Antarctica Peninsula. *Earth Surface Processes Landforms* 33, 503–512.
- Applegate, P.J., Urban, N.M., Keller, K., Lowell, T.V., Laabs, B.J.C., Kelly, A.M., Alley, R.B., 2012. Improved moraine age interpretations through explicit matching of geomorphic process models to cosmogenic nuclide measurements from single landforms. *Quaternary Research* 77, 293–304.
- Balco, G., Stone, J.O., Lifton, N.A., Dunai, T.J., 2008. A complete and easily accessible means of calculating surface exposure ages or erosion rates from ^{10}Be and ^{26}Al measurements. *Quat. Geochronol.* 3 (3), 174–195. <https://doi.org/10.1016/j.quageo.2007.12.001>.
- Barnard, A., Wellner, J.S., Anderson, J.B., 2014. Late Holocene climate change recorded in proxy records from a bransfield basin sediment core, Antarctic Peninsula. *Polar Res.* 33 (1), 17236. <https://doi.org/10.3402/polar.v33.17236>.
- Batchelor, C.I., Downdeswell, J.A., Hogan, K.A., Larer, R.D., Parsons, E., West, O., 2019. Processes and patterns of glacier-influenced sedimentation and recent tidewater glacier dynamics in Darbel Bay, Western Antarctic Peninsula. *Antarct. Sci.* 31 (4), 218–227. <https://doi.org/10.1017/S0954102019000191>.
- Bentley, M.J., Fogwill, C.J., Kubik, P.W., Sugden, D.E., 2006. Geomorphological evidence and cosmogenic Be-10/Al-26 exposure ages for the Last Glacial Maximum and deglaciation of the Antarctic Peninsula ice sheet. *Geol. Soc. Am. Bull.* 118, 1149–1159. <https://doi.org/10.1130/B25735.1>.
- Bentley, M.J., Hodgson, D.A., Smith, J.A., Cox, N.J., 2005b. Relative sea level curves for the south shetland islands and marguerite Bay, Antarctic Peninsula. *Quat. Sci. Rev.* 24 (10–11), 1203–1216.
- Bentley, M.J., Hodgson, D.A., Sugden, D.A., Roberts, S.J., Smith, J.A., Leng, M.J., Bryant, C., 2005a. Early Holocene retreat of George VI Ice Shelf, Antarctic Peninsula. *Geology* 33, 173–176.
- Bentley, M.J., Johnson, J.S., Hodgson, D.A., Dunai, T., Freedman, S.P.H.T., Ó Cofaigh, C., 2011. Rapid deglaciation of Marguerite Bay, Western Antarctic Peninsula in the early Holocene. *Quat. Sci. Rev.* 30 (23–24), 3338–3349.
- Bertler, N.A.N., Mayewski, P.A., Carter, L., 2011. Cold conditions in Antarctica during the Little Ice Age — implications for abrupt climate change mechanisms. *Earth Planet Sci. Lett.* 308, 41–51. <https://doi.org/10.1016/j.epsl.2011.05.021>.
- Björck, S., Hakansson, H., Zale, R., Karlén, W., Jonsson, B.L., 1991. A late Holocene Lake sediment sequence from Livingston Island, South Shetland Islands, with palaeoclimatic implications. *Antarct. Sci.* 3, 61–72.
- Björck, S., Hjort, C., Ingólfsson, O., Zale, R., Sing, J., 1996. Holocene deglaciation chronology from Lake sediments. In: Lopez-Martinez, J., Thomson, M.R.A., et al. (Eds.), *Geomorphological Map of Byers Peninsula*. Livingston Island. BAS GEOMAP Series, Sheet 5-a, I: 25 000, with Supplementary Text. British Antarctic Survey, Cambridge, p. 65.
- Birkemajer, K., 1981. Lichenometric dating of raised marine beaches at admiralty Bay, King George Island (South Shetland Islands, west Antarctica). *Bulletin de l'Académie Polonaise des Sciences* 29, 119–127.
- Blanckenburg, F., 2005. The control mechanisms of erosion and weathering at basin scale from cosmogenic nuclides in river sediment. *Earth Planet Sci. Lett.* 237, 462–479.
- Čejka, T., Nývlt, D., Kopalová, K., Bulínová, M., Kavan, J., Lirio, J.M., Coria, S.H., van de Vijver, B., 2020. Timing of the neoglacial onset on the north-eastern Antarctic Peninsula based on lacustrine archive from Lake Anónima, Vega island. *Glob. Planet. Change* 184, 103050. <https://doi.org/10.1016/j.gloplacha.2019.103050>.
- Çiner, A., Sarıkaya, M.A., Yıldırım, C., 2017. Misleading old age on a young landform? The dilemma of cosmogenic inheritance in surface exposure dating: moraines vs. rock glaciers. *Quat. Geochronol.* 42, 76–88. <https://doi.org/10.1016/j.quageo.2017.07.003>.
- Çiner, A., Yıldırım, C., Sarıkaya, M.A., Seong, Y.B., Byung, Y.Y., 2019. ^{10}Be cosmogenic dating of glacial erratic boulders on Horseshoe Island in Western Antarctic Peninsula confirms the rapid deglaciation in early Holocene. *Antarct. Sci.* 31 (6), 319–331. <https://doi.org/10.1017/S0954102019000439>.
- Christ, A.J., Talaia-Murray, M., Elking, N., Domack, E.W., Leventer, A., Lavoie, C., Petrushak, S., 2015. Late Holocene glacial advance and ice shelf growth in Bariliari Bay, Graham land, west Antarctic Peninsula. *GSA Bulletin* 127 (1–2), 297–315. <https://doi.org/10.1130/B31035.1>.
- Clapperton, C.M., Sugden, D.E., 1988. Holocene glacier fluctuations in South America and Antarctica. *Quat. Sci. Rev.* 7, 185–198.

- Cook, A.J., Fox, A.J., Vaughan, D.G., Ferringo, J.G., 2005. Retreating glacier fronts on the Antarctic Peninsula over the past half-century. *Science* 308, 541–544.
- Cook, A.J., Holland, P.R., Meredith, M.P., Murray, T., Luckman, A., Vaughan, D.G., 2016. Ocean forcing of glacier retreat in the Western Antarctic Peninsula. *Science* 15, 283–286.
- Curl, J.E., 1980. A glacial history of the South Shetland Islands, Antarctica. In: Institute of Polar Studies Report, vol. 63. Institute of Polar Studies, Ohio State University, Columbus, p. 129.
- Dalaïden, Q., Goosse, H., Klein, F., Lenaerts, J.T.M., Holloway, M., Sime, L., Thomas, E. R., 2020. How useful is snow accumulation in reconstructing surface air temperature in Antarctica? A study combining ice core records and climate models. *Cryosphere* 14, 1187–1207.
- Davies, B.J., Golledge, N.R., Glasser, N.F., Carrivick, J.L., Ligtenberg, S.R.M., Barrand, N. E., van de Broeke, M.R., Hambrey, M.J., Smellie, J.L., 2014. Modelled glacier response to Centennial temperature and precipitation trends on the Antarctic Peninsula. *Nat. Clim. Change* 4, 993–998.
- Davies, B.J., Hambrey, M.J., Glasser, N.F., Holt, T., Rodes, A., Smellie, J.L., Blockley, S. P., 2017. Ice-dammed lateral Lake and episize Lake insights into Holocene dynamics of Marguerite Trough Ice Stream and George VI ice shelf, Alexander Island, Antarctic Peninsula. *Quat. Sci. Rev.* 177, 189–219. <https://doi.org/10.1016/j.quascirev.2017.10.016>.
- Domack, E.W., Ishman, S.E., Stein, A.B., McClenen, C.E., Jull, A.J.T., 1995. Late Holocene advance of the Muller ice shelf, Antarctic Peninsula – sedimentological, geochemical and paleontological evidence. *Antarct. Sci.* 7, 159–170.
- Domack, E.W., Leventer, A., Dunbar, G.B., Taylor, F., Brachfeld, S., Sjønneskog, C., Party, O.L.S., 2001. Chronology of the palmer deep site, Antarctic Peninsula: a Holocene palaeoenvironmental reference for the circum-Antarctic. *Holocene* 11, 1–9.
- Fernández-Fernández, J.M., Oliva, M., Palacios, D., García-Oteyza, J., Navarro, F., Schimmelpfennig, I., Léannid, L., ASTER Team, 2021. Ice thinning on nunataks during the last glacial termination in the Antarctic Peninsula according to cosmic-ray exposure dating: evidence and uncertainties. *Quat. Sci. Rev.* 264, 107029.
- García, M., Dowdeswell, J.A., Noormets, R., Hogan, K.A., Evans, J., ÓCofaigh, C., Larer, R.D., 2016. Geomorphology and shallow-acoustic investigation of an Antarctic Peninsula fjord system using high resolution ROV and shipboard geophysical observations: ice dynamics and behaviour since the Last Glacial Maximum. *Quat. Sci. Rev.* 153, 122–138. <https://doi.org/10.1016/j.quascirev.2016.10.014>.
- Giralt, S., Hernández, A., Pla-Rabés, S., Antoniades, D., Toro, M., Granados, I., Oliva, M., 2020. Holocene environmental changes deduced from lake sediments. In: Oliva, M., Ruiz-Fernández (Eds.), *Past Antarctica*. Elsevier, pp. 51–68.
- Guglielmin, M., Convey, P., Malfassi, F., Cannone, N., 2016. Glacial fluctuations since the medieval warm period at Rothera point (Western Antarctic Peninsula). *Holocene* 26 (1), 154–158. <https://doi.org/10.1177/0959683615596827>.
- Hall, B.L., 2007. Late-holocene advance of the collins ice cap, King George Island, South Shetland Islands. *Holocene* 17, 1253–1258.
- Hall, B.L., 2010. Holocene relative sea-level changes and ice fluctuations in the South Shetland Islands. *Global Planet. Change* 74, 15–26.
- Hall, B.L., Perry, E.R., 2004. Variations in ice rafted detritus on beaches in the South Shetland Islands: a possible climate proxy. *Antarct. Sci.* 16 (3), 339–344. <https://doi.org/10.1017/S0954102004002147>.
- Hein, A.S., Fogwill, C.J., Sugden, D.E., Xu, S., 2014. Geological scatter of cosmogenic-nuclide exposure ages in the Shackleton Range, Antarctica: implications for glacial history. *Quat. Geochronol.* 19, 52–66.
- Heredia-Barión, P., Roberts, S.J., Spiegel, C., Binnie, S.A., Wacker, L., Davies, J., Gabriel, I., Jones, V.J., Blockley, S., Pearson, E.J., Foster, L., Davies, S.J., Roland, T. P., Hocking, E.P., Bentley, M.J., Hodgson, D.A., Hayward, C.L., McCulloch, R.D., Strelin, J.A., Kuhn, G., 2023a. Holocene deglaciation and glacier readvances on the Fildes Peninsula and King George Island (Isla 25 de Mayo), South Shetland Islands, NW Antarctic Peninsula. *Holocene* 33, 636–658. <https://doi.org/10.1177/09596836231157059>.
- Heredia-Barión, P., Strelin, J.A., Roberts, S.J., Spiegel, C., Wacker, L., Niedermann, S., Bentley, M.J., Pearson, E.J., Czalbowski, N.T.M., Davies, S.J., Schnetger, B., Grosjean, M., Arcusa, S., Perren, B., Hocking, E.P., Kuhn, G., 2023b. The impact of Holocene deglaciation and glacial dynamics on the landscapes and geomorphology of potter peninsula, king george island (Isla 25 Mayo), NW Antarctic Peninsula. *Front. Earth Sci.* 10, 1073075. <https://doi.org/10.3389/feart.2022.1073075>.
- Heyman, J., Stroeve, A.P., Harbor, J.M., Caffee, M.W., 2011. Too young or too old: evaluating cosmogenic exposure dating based on an analysis of compiled boulder exposure ages. *Earth Planet. Sci. Lett.* 302, 71–80.
- Hodgson, D.A., Roberts, S.J., Smith, J.A., Verleyen, E., Sterken, M., Labarque, M., Sabbe, K., Vyverman, W., Allen, C.S., Leng, M.J., Bryant, C., 2013. Late Quaternary environmental changes in Marguerite Bay, Antarctic Peninsula, inferred from lake sediments and raised beaches. *Quat. Sci. Rev.* 68, 216–236.
- IPCC, 2019. In: Shukla, P.R., Skea, J., Calvo Buendia, E., Masson-Delmotte, V., Pörtner, H.-O., Roberts, D.C., Zhai, P., Slade, R., Connors, S., van Diemen, R., Ferriat, M., Haughey, E., Luz, S., Neogi, S., Pathak, M., Petzold, J., Portugal Pereira, J., Vyas, P., Huntley, E., Kissick, K., Belkacemi, M., Malley, J. (Eds.), *Climate Change and Land: Special Report on Climate Change, Desertification, Land Degradation, Sustainable Land Management, Food Security, and Greenhouse Gas Fluxes in Terrestrial Ecosystems*, 864p.
- ICE-D. Informal cosmogenic-nuclide exposure-age database. <https://ice-d.apps.pgc.umn.edu/antarctica/>.
- Ingólfsson, Ó., Hjort, C., Berkman, P.A., Björck, S., Colhoun, E., Goodwin, I.D., Hall, B., Hirakawa, K., Melles, M., Moller, P., Prentice, M.L., 1998. Antarctic glacial history since the Last Glacial Maximum: an overview of the record on land. *Antarct. Sci.* 10, 326–344.
- Ingólfsson, Ó., Hjort, C., Humlum, O., 2003. Glacial and climate history of the Antarctic Peninsula since the Last Glacial Maximum. *Arctic Antarct. Alpine Res.* 35 (2), 175–186.
- John, B.S., Sugden, D.E., 1971. Raised marine features and phases of glaciation in the South Shetland Islands. *Br. Antarct. Surv. Bull.* 24, 45–111.
- Johnson, J.S., Everest, J.D., Leat, P.T., Golledge, N.R., Rood, D.H., Stuart, F.M., 2012. The deglacial history of NW Alexander Island, Antarctica, from surface exposure dating. *Quaternary Research* 77, 273–280. <https://doi.org/10.1016/j.yqres.2011.11.012>.
- Kilfeather, A.A., Ó Cofaigh, C., Lloyd, J.M., Dowdeswell, J.A., Xu, S., Moreton, S., 2011. Ice-stream retreat and ice-shelf history in Marguerite trough, Antarctic Peninsula: sedimentological and foraminiferal signatures. *Geol. Soc. Am. Bull.* 123, 997–1015.
- Khim, B.K., Yoon, H.I., Kang, C.Y., Bahk, J.J., 2002. Unstable climate oscillations during the late Holocene in the eastern Barnebasin, Antarctic Peninsula. *Quat. Res.* 58, 234–245. <https://doi.org/10.1006/qres.2002.2371>.
- Kim, E., Seong, Y.B., Rhee, H.H., Khadsuren, P., Yu, B.Y., Eliades, J., 2024. Cosmogenic ^{10}Be research: standard reference materials and blank analysis. *J. of the Korean Earth Science Society* 45 (6), 624–636. <https://doi.org/10.5467/JKESS.2024.45.6.624>.
- Kohl, C.P., Nishizumi, K.K., 1992. Chemical isolation of quartz for measurement of *in-situ*-produced cosmogenic nuclides. *Geochem. Cosmochim. Acta* 56 (9), 3583–3587.
- Köse, O., Sarikaya, M.A., Çiner, A., Candaş, A., Yıldırım, C., 2022. Late Quaternary glaciations and cosmogenic ^{36}Cl geochronology of Mount Karanfil, taurus Mountains, Turkey. *Quat. Sci. Rev.* 291. <https://doi.org/10.1016/j.quascirev.2022.107656>.
- Lifton, N., Sato, T., Dunai, T.J., 2014. Scaling in situ cosmogenic nuclide production rates using analytical approximations to atmospheric cosmic-ray fluxes. *Earth Planet. Sci. Lett.* 386, 149–160.
- Li, Y., Cole-Dai, J., Zhou, L., 2009. Glaciogenic evidence in an east Antarctica ice core of a recent (AD 1450–1850) neoglacial episode. *J. Geophys. Res.* 114, D08117.
- Liu, X., Sun, L., Xie, Z., Yin, X., Wang, Y.A., 2005. 1300-year record of penguin populations at Ardley Island in the Antarctic, as deduced from the geochemical data in the ornithogenic lake sediments. *Arctic Antarct. Alpine Res.* 37, 490–498.
- Livingstone, S.J., O'Cofaigh, C., Stokes, C.R., Hillenbrand, C.-D., Vieli, A., Jamieson, S.S. R., 2013. Glacial geomorphology of Marguerite Bay palaeo-ice stream, Western Antarctic Peninsula. *J. Maps* 9 (4), 558–572.
- Loske, W., Herve, F., Miller, H., Pankhurst, R.J., 1997. Rb-Sr and U-Pb studies of the pre-andean and andean magmatism in the Horseshoe Island Area, Marguerite Bay (Antarctic Peninsula). In: Ricci, C.A. (Ed.), *The Antarctic Region: Geological Evolution and Processes*. Terra Antartica Publication, Siena, pp. 353–360.
- Mann, M., Bradley, R., Hughes, M., 1998. Global-scale temperature patterns and climate forcing over the past six centuries. *Nature* 392, 779–787. <https://doi.org/10.1038/33859>.
- Matthews, D.W., 1983. The geology of Horseshoe and Lagotellerie islands, Marguerite Bay, Graham Land. *Br. Antarct. Surv. Bull.* 52, 125–154.
- Miller, G.H., Geirsdóttir, A., Zhong, Y., et al., 2012. Abrupt onset of the Little Ice Age triggered by volcanism and sustained by sea-ice/ocean feedbacks. *Geophys. Res. Lett.* 39, L02708. <https://doi.org/10.1029/2011GL050168>.
- Molina, C., Navarro, F.J., Calvet, J., García-Sellés, D., Lapazaran, J.J., 2007. Hurd Peninsula glaciers, Livingston Island, Antarctica, as indicators of regional warming: ice-volume changes during the period 1956–2000. *Ann. Glaciol.* 46, 43–49. <https://doi.org/10.3189/172756407782871765>.
- Ó Cofaigh, C., Davies, B.J., Livingstone, S.J., Smith, J.A., Johnson, J.S., Hocking, E.P., Hodgson, D.A., Anderson, J.B., Bentley, M.J., Canals, M., Domack, E., Dowdeswell, J. A., Evans, J., Glasser, N.F., Hillenbrand, C.-D., Larer, R.D., Roberts, S.J., Simms, A. R., 2014. Reconstruction of ice-sheet changes in the Antarctic Peninsula since the Last Glacial Maximum. *Quat. Sci. Rev.* 100, 87–110.
- Ó Cofaigh, C., Dowdeswell, J.A., Evans, J., Larer, R.D., 2008. Geological constraints on Antarctic palaeo-ice stream retreat. *Earth Surf. Process. Landf.* 33, 513–525.
- Oliva, M., Antoniades, D., Giralt, S., Granados, I., Pla-Rabes, S., Toro, M., Liu, E.J., Sanjurjo, J., Vieira, G., 2016. The Holocene deglaciation of the Byers Peninsula (Livingston Island, Antarctica) based on the dating of lake sedimentary records. *Geomorphology* 261, 89–102. <https://doi.org/10.1016/j.geomorph.2016.02.029>.
- Oliva, M., Navarro, F.J., Hrbáček, F., Hernández, A., Nývlt, D., Pereira, P., Ruiz-Fernández, J., Trigo, R., 2017. Recent regional cooling of the Antarctic Peninsula and its impacts on the cryosphere. *Sci. Total Environ.* 580, 210–223. <https://doi.org/10.1016/j.scitotenv.2016.12.030>.
- Oliva, M., Palacios, D., Fernández-Fernández, J.M., Fernandes, M., Schimmelpfennig, I., Vieira, G., Antoniades, D., Pérez-Alberti, A., García-Oteyza, J., Team, A., 2023. Holocene deglaciation of the northern Fildes Peninsula, King George Island, Antarctica. *Land Degrad. Dev.* 34, 3973–3990.
- Oliva, M., Palacios, D., Sancho, L.G., Fernández-Fernández, J.M., Ciner, A., García-Oteyza, J., Sarikaya, M.A., Serrano, E., Kaveh-Firouz, A., Pérez-Alberti, A., Schimmelpfennig, I., Vieira, G., Antoniades, D., Pérez-Alberti, A., García-Oteyza, J., Team, A., 2024. The origin of ice-free areas of the Hurd Peninsula (Livingston Island, Antarctica). *Quat. Sci. Rev.* 344. <https://doi.org/10.1016/j.quascirev.2024.108991>.
- Orsi, A.J., Cornuelle, B.D., Severinghaus, J.P., 2012. Little Ice Age cold interval in west Antarctica: evidence from borehole temperature at the west Antarctic ice sheet (WAIS) divide. *Geophys. Res. Lett.* 39, L09710.
- Palacios, D., Ruiz-Fernández, J., Oliva, M., Andrés, N., Fernández-Fernández, J.M., Schimmelpfennig, I., Leanni, L., González-Díaz, B., 2020. Timing of formation of neoglacial landforms in the South Shetland Islands (Antarctic Peninsula): regional and global implications. *Quat. Sci. Rev.* 234, 106248. <https://doi.org/10.1016/j.quascirev.2020.106248>.

- Porter, S., 2001. Onset of neoglaciation in the southern hemisphere. *J. Quaternary Science* 15 (4), 395–408.
- Putkonen, J., Swanson, T., 2003. Accuracy of cosmogenic ages for moraines. *Quaternary Research* 59, 255–261.
- Reilly, B.T., Natter, C.J., Brachfeld, S.A., 2016. Holocene glacial activity in Barilari Bay, West Antarctic Peninsula, tracked by magnetic mineral assemblages: linking ice, ocean, and atmosphere. *Geochem., Geophys., Geosyst.* 17 (11), 4553–4565. <https://doi.org/10.1002/2016GC006627>.
- Renssen, H., Seppä, H., Crosta, X., Goosse, H., Roche, D.M., 2012. Global characterization of the Holocene Thermal Maximum. *Quat. Sci. Rev.* 48, 7–19. <https://doi.org/10.1016/j.quascirev.2012.05.022>.
- Renssen, H., Seppä, H., Heiri, O., Roche, D.M., Goosse, H., Fichefet, T., 2009. The spatial and temporal complexity of the Holocene Thermal Maximum. *Nat. Geosci.* 2, 411–414.
- Repka, J.L., Anderson, R.S., Finkel, R.C., 1997. Cosmogenic dating of fluvial terraces, Fremont river, Utah. *Earth Planet Sci. Lett.* 152 (1–4), 59–73.
- Roman, M., Piskova, A., Sanderson, D.C.W., Cresswell, A., et al., 2024. The late Holocene deglaciation of James Ross Island, Antarctic Peninsula: OSL and 14C-dated multi-proxy sedimentary record from Monolith Lake. *Quat. Sci. Rev.* 333. <https://doi.org/10.1016/j.quascirev.2024.108693>.
- Sarıkaya, M.A., Çiner, A., Yıldırım, C., 2017. A new sampling strategy for cosmogenic surface exposure dating of moraines: Amalgamated Boulder Chips (ABCs). 19th EGU General Assembly 3939, 23–28 April 2017, Vienna.
- Sarıkaya, M.A., Çiner, A., Yıldırım, C., Parnikoza, I., Seong, Y.B., Yu, B.Y., Wilcken, K., 2025. Cosmogenic exposure age record of emerged nearshore erratic boulders on the Western Antarctic Peninsula. *Antarct. Sci.* <https://doi.org/10.1017/S0954102025100394>.
- Shevenell, A.E., Domack, E.W., Kernan, G.M., 1996. Record of Holocene palaeoclimate change along the Antarctic Peninsula: evidence from glacial marine sediments, Lallemand fjord. *Pap. Proc. R. Soc. Tasman.* 130, 55–64.
- Simkins, L.M., Simms, A.R., Dewitt, R., 2013. Relative sea-level history of Marguerite Bay, Antarctic Peninsula derived from optically stimulated luminescence-dated beach cobbles. *Quat. Sci. Rev.* 77, 141–155.
- Simms, A., Bentley, M.J., Simkins, L.M., Zurbuchen, J., Reynolds, L.C., DeWitt, R., Thomas, E.R., 2021. Evidence for a “Little Ice Age” glacial advance within the Antarctic Peninsula - examples from glacially-overrun raised beaches. *Quat. Sci. Rev.* <https://doi.org/10.1016/j.quascirev.2021.107195>.
- Simms, A.R., Ivins, E.R., DeWitt, R., Kouremenos, P., Simkins, L.M., 2012. Timing of the most recent neoglacial advance and retreat in the South Shetland Islands, Antarctic Peninsula: insights from raised beaches and Holocene uplift rates. *Quat. Sci. Rev.* 47, 41–55.
- Smith, I.F., 1973. Gravity survey on Shoesmith glacier, Horseshoe Island, Graham Land. *Br. Antarct. Surv. Bull.* 33 (and 34), 77–82.
- Suda, C.N.K., Vani, G.S., Oliveira, M.J., Rodrigues, E., Rodrigues, E., Lavrado, H.P., 2015. The biology and ecology of the Antarctic limpet *Nacella concinna*. *Polar Biol.* <https://doi.org/10.1007/s00300-015-1789-6>.
- Swanger, K., Lamp, J.L., Schaefer, J.M., Winckler, G., Schimmelpfennig, I., ASTER Team, 2024. Pleistocene glacial advances and exposure age scatter in the Olympus range, Antarctica: a study of cosmogenic $^{36}\text{Cl}/^{3}\text{He}$ in dolerites and ^{10}Be in sandstones. *Quat. Geochronol.* 85. <https://doi.org/10.1016/j.quageo.2024.101632>.
- Taylor, F., Sjuneskog, C., 2002. Postglacial marine diatom record of the Palmer Deep, Antarctic Peninsula (ODP leg 178, site 1098) 2. Diatom assemblages. *Paleoceanography* 17. <https://doi.org/10.1029/2000PA000564>.
- Tükenmez, E., Gülder, E., Kaya, Ö., Polat, H.F., 2022. Bathymetric analysis of Lystad Bay, Horseshoe Island by using high resolution multibeam echosounder data. *J. of Naval Sciences and Engineering, Oceanography and Hydrography* 18 (2), 281–303.
- Turner, J., Barrand, N.E., et al., 2014. Antarctic climate change and the environment: an update. *Polar Rec.* 50 (254), 237–259. <https://doi.org/10.1017/S0032247413000296>.
- Turner, J., Marshall, G., Clem, K., Colwell, S., Phillips, T., Lu, H., 2020. Antarctic temperature variability and change from station data. *Int. J. of Climatology* 40 (6), 2986–3007. <https://doi.org/10.1002/joc.6378>.
- Vaughan, D.G., Marshall, G.J., Connolley, W.M., Parkinson, C., Mulvaney, R., Hodgson, D.A., King, J.C., Pudsey, C.J., Turner, J., 2003. Recent rapid regional climate warming on the Antarctic Peninsula. *Clim. Change* 60, 243–274.
- Velev, S., Lazarova, A., Karaoglan, F., Vassilev, O., Selbesoglu, M.O., 2023. Early Jurassic and Late Cretaceous magmatism on Horseshoe Island, Antarctic Peninsula: New U-Pb and microstructural data. *Geol. Balc.* 52 (3), 29–32. <https://doi.org/10.52321/GeolBalc.52.3.29>.
- Warner, N.R., Domack, E.W., 2002. Millennial-to decadal-scale paleoenvironmental change during the Holocene in the Palmer deep, Antarctica, as recorded by particle size analysis. *Paleoceanography* 17. <https://doi.org/10.1029/2000PA000602>.
- Wassell, A., Håkansson, H., 1992. Diatom stratigraphy in a lake on Horseshoe Island, Antarctica: a marine-brackish-fresh water transition with comments on the systematics and ecology of the most common diatoms. *Diatom Res.* 7 (1), 157–194.
- Wetterauer, K., Scherler, D., Anderson, L.S., Wittmann, H., 2022. Temporal evolution of headwall erosion rates derived from cosmogenic nuclide concentrations in the medial moraines of glacier d’Otemma, Switzerland. *Earth Surf. Process. Landf.* 47 (10), 2437–2454.
- Yıldırım, C., 2020. Geomorphology of Horseshoe Island, Marguerite Bay, Antarctica. *J. Maps* 16 (2), 56–67. <https://doi.org/10.1080/17445647.2019.1692700>.
- Yıldırım, C., Çiner, A., Sarıkaya, M.A., Hiday, A., 2024. Cosmogenic surface exposure (^{10}Be) dating of raised beaches in Marguerite Bay, Antarctic Peninsula: implications for relative sea level curve. *Quat. Sci. Rev.* 344. <https://doi.org/10.1016/j.quascirev.2024.108995>.
- Yu, Z., Beilman, D.W., Loisel, J., 2016. Transformations of landscape and peat-forming ecosystems in response to late Holocene climate change in the Western Antarctic Peninsula. *Geophys. Res. Lett.* 43, 7186–7195.